CSIRO MARINE LABORATORIES
Report 231

Tests of mixed-layer schemes and surface boundary conditions in an Ocean General Circulation Model, using the IMET flux data set

J. S. Godfrey and A. Schiller

1997

Godfrey, J. S.
Tests of mixed-layer schemes and surface boundary conditions in an ocean general circulation model, using the IMET flux data set.

ISBN 0 643 06157 6.

1. Ocean-atmosphere interaction - Measurement.
2. Ocean temperature - Measurement.
   I. Schiller, Andreas, 1960 - .
   II. CSIRO. Division of Marine Research.
   III. Title. (Series : Report (CSIRO. Marine Laboratories) ; no. 231)

551.4601

CONTENTS

ABSTRACT

The four-month long data series of accurate surface fluxes from the IMET meteorological buoy, deployed from November 1992 – February 1993 in the equatorial west Pacific, is used to test versions of the mixed-layer scheme of Chen et al. (1994a), as adapted by Power et al. (1995) for use in the MOM Ocean General Circulation Model (OGCM). The scheme combines an estimate of the mixed-layer depth similar to that of Niiler and Kraus (1977) with the Richardson number-dependent mixing of Pacanowski and Philander (1981). Predicted temperature and salinity evolution is very similar to that found by Weller and Anderson (1996), using the Price et al. (1986) scheme. Both schemes are quite successful at simulating observed Sea Surface Temperatures (SSTs) over the observation period, except during a prolonged wind burst when observed SSTs decreased faster than predicted by either scheme. Both models predict density-based mixed-layer depths that agree quite well with observations; the errors in predicting SST have recently been shown to be due to horizontal advection, unresolved in these 1-D models (Feng et al., 1997).

In a second test of the Power et al. scheme, the Niiler-Kraus mixed-layer depth was set to zero, so that only the Pacanowski-Philander shear-dependent mixing operated. The results were very similar to the first run: i.e. at the low latitude of the IMET mooring, mixing was dominated by shear instability, even during westerly wind bursts.

To examine this rather surprising result further, we made runs with identical fluxes, but at higher latitudes. Coriolis effects were expected to progressively limit the velocity shears and increase the Richardson numbers, and hence to reduce the magnitude of the shear-driven mixing compared to the Niiler-Kraus mixing. This in fact occurred, but even at 20° from the equator, shear-driven mixing still dominated. However, even over the strongest wind burst—that of 13 December 1992-3 January, 1993—the mean wind stress $\rho_a u^{*2}$ was less than 0.1 N/m^2. By comparison, winter mean stresses exceed 0.2 N/m^2 in parts of the high-latitude oceans. The deepening of the Niiler-Kraus mixed-layer depth is mainly controlled by u^{*3}, for high winds. It therefore seems likely that the reason the mixed-layer depth tends to be controlled by the Niiler-Kraus term at high latitudes is that the values of u^{*3} found there are large, rather than that Coriolis effects reduce shear instability.

The net error in the IMET data series is estimated to be less than about 10 W/m^2. To test the effect of such an error on the model's predictions, the Chen et al. scheme was run with 10 W/m^2 added to the basic IMET net heat flux. The SST increased by about 0.5°C over the first 30 days, but surprisingly, the temperature difference equilibrated after this time. This occurred because the increased heat flux reduced the mixed-layer depth slightly; transparency caused the excess heat to be trapped just below the mixed layer, and a greater fraction of the buoyancy input into the mixed layer was taken up by freshwater input. This provides a negative-feedback mechanism which may partly control the SST over the Warm Pool region. The result also suggests that the discrepancies between modelled and observed SSTs are as likely to be due to residual flux errors as to problems in mixed-layer formulation.

In the second part of the Report, we review literature on surface heat flux boundary conditions, introduce our own, and describe a partial test of that boundary condition with IMET data. The standard Seager et al. (1988) parametrisation results in very good SST simulation when observed wind speeds and shortwave radiation are used. However, if IMET wind speeds are reduced by 20% and shortwave radiation increased by 10%—typical of errors in available

products—SST increases by about 2.5°C. Use of our proposed flux correction technique reduces the error to 0.5°C. Replacement of shortwave radiation by its daily average value makes very little difference to modelled daily average SST.

1. INTRODUCTION

A crucial element of any successful model for forecasting interannual changes in the earth's coupled climate system will be an ability to accurately forecast changes in Sea Surface Temperature (SST), given good estimates of surface fluxes of heat, freshwater and momentum. While good representation of large-scale ocean dynamics is helpful for predicting SSTs, it is not enough; one must also represent mixed-layer processes accurately.

The first concern of this Report (Sections 2-6) is to describe the results of tests of two mixed-layer schemes, using accurately known fluxes, temperatures and salinities from the Woods Hole Oceanographic Institution IMET mooring. This was deployed at (1°45'S, 156°E) from October 1992 to March 1993, to cover the TOGA-COARE experiment.

While having an accurate mixed-layer model is essential, a further problem for climate modelling is that in practice our estimates of the surface heat fluxes are too inaccurate to use them directly for modelling the SST. The problem of parameterising the surface heat fluxes in an OGCM has received considerable attention recently (e.g. Haney 1971, Seager et al. 1988, Chen et al. 1994b, Seager and Blumenthal 1994, Kleeman and Power 1995, Syu et al. 1995, Ji et al. 1995). In the second part of this report (Section 7) we review this literature, and outline our choice of surface heat flux boundary condition. S. Wijffels (pers. comm.) suggested we could test this boundary condition, with the IMET data series; we discuss these tests in Section 7. However, we can only test some aspects of the boundary condition, so the discussion is brief.

The Report is more detailed than is usual in published papers. However, we need to be sure, for our own planning purposes and for future documentation, that all participants understand the physical basis of the model in detail. We have therefore decided to write this and possibly other reports about the LWRRDC Project, to deal with some of the topics that usually get inadequate treatment.

2. THE MIXED-LAYER SCHEMES

The first mixed-layer scheme considered here is that of Power et al. (1995), who adapted the mixed-layer model of Chen et al. (1994a)—originally designed for an OGCM that explicitly resolved a mixed-layer of variable depth—for use in the Geophysical Fluid Dynamics Laboratory Modular Ocean Model (MOM). The MOM model contains levels of fixed depths, so Power et al. had to make some fairly major, if technical, changes to the original code to incorporate the Chen et al. concept in the MOM scheme. We refer to the result as the "Chen-Power scheme". Power et al. did not rigorously test their revised model against observations; we have undertaken further testing and tuning of the Chen-Power scheme.

The second scheme tested is a modification of the first, in which the Niiler-Kraus element of the Power et al. scheme is removed (by setting the Kraus mixed-layer depth at zero). The result is quite close to the mixing scheme of Price et al. (1986), (referred to below as the Price scheme), because mixing is then controlled solely by Richardson-number dependent effects as in Price et al. We refer to the model obtained by setting the Kraus depth to zero as the "modified Price scheme".

The Chen scheme was designed to incorporate the best features of the Price scheme and of the Niiler-Kraus (1979) scheme. The Price scheme assumes that mixing is dominated by shear instability and convection; it performs very well when the net upward buoyancy flux B_0 is negative (i.e. the surface is being warmed and/or freshened), and winds are light to moderate (e.g. Price et al. 1986). The Niiler-Kraus (1979) scheme is more successful in conditions of prolonged positive B_0 and strong winds, as found in winter in high-latitude oceans (e.g. Davis et al. 1981).

The IMET time series contains quite long consecutive periods in which each kind of condition prevailed. It is therefore at least plausible that the IMET time series should provide a convenient overall testbed for any mixed-layer scheme. Weller and Anderson (1996) have already shown that, while the Price scheme did extremely well in simulating changes in SST during the light-wind, negative B_0 periods of the IMET data series, it underestimated SST loss during strong-wind, positive B_0 periods ("westerly wind bursts").

In Sections 3-6 below we report on tests of whether the Chen-Power scheme and the modified Price scheme did as well as or better than the Price simulation reported by Weller and Anderson (1996), and describe some technical issues involved in mixed-layer modelling in a MOM-type model. Section 3 describes the physics of the Chen scheme; Section 4 deals with numerical details; Section 5 describes the observed IMET fluxes, while Section 6 is reports the results of 1-D model tests.

3. THE CHEN-POWER ET AL. MIXING SCHEME

Although this scheme has been described by Power et al., we describe it in detail here, to give readers a better qualitative "feel" for how it works. Chen et al. (1994a) loosely follow Niiler and Kraus (1977). Thus they assume that eddy viscosity and diffusivity is large within a mixed-layer of depth h_K (referred to below as the "Kraus depth"). In absence of advection—and provided the RHS of (1) is positive—they assume the entrainment rate $w_e (= \partial h_K / \partial t$, in our 1-D application) obeys "the simplified bulk turbulent energy equation":

$$\begin{aligned}&(b_1 - b_2)h_K\, w_e = \\ &= (b_1 - b_2)h_K \partial h_K / \partial t = 2m_0(u^{*3}) + h_K[(1+n_0)B_0 - (1-n_0)|B_0|]/2 \\ &+ J_0[h(1+\exp(-h_K/h_B)) - 2h_B(1-\exp(-h_K/h_B))]\end{aligned} \tag{1}$$

$$\begin{aligned}&= 2m_0(u^{*3}) + h_K B_0 - (1-n_0)h_K(|B_0|+B_0)/2 \\ &+ J_0[h_K(1+\exp(-h_K/h_B)) - 2h_B(1-\exp(-h_K/h_B))]\end{aligned} \tag{1'}$$

Niiler and Kraus' eg. (10.30) coincides with (1), (1'), in the limit of infinite h_K / h_B, except that their LHS is replaced by: $[(b_1 - b_2)h_K - sv^2]\, w_e$. The extra term in $-sv^2$ accounts for turbulent KE production by shears at the mixed-layer base. Chen et al. ignore this term, since the Richardson-number-dependent mixing is accounted for separately in their model (see below). Here b_1, b_2 are the buoyancies of water in the mixed-layer, and just below it. B_0 is the upward surface buoyancy flux (i.e. it is positive when the ocean is losing buoyancy), and u^* is the friction velocity (in water). B_0 is given by:

$$B_0 = (\alpha g / \rho C_p)[R_0 - I_0 + E_0 + H_0] + (\beta g S_0)(E_0 / L_E - P) \tag{2}$$

where R_0 is the net *upward total* radiation at the surface (usually strongly negative by day, weakly positive by night), while E , H_0 are the latent and sensible heat fluxes at the surface (generally positive). $I_0 = 0.45\,R_s$ is the penetrating component of the *shortwave* influx, R_s ; I_0 is negative. C_p is the specific heat of water and ρ its density; and in (1), (1'), $J_0 = \alpha g I_0 / \rho C_p$. S_0 is a mean surface salinity (about 35 psu), L_E the latent heat of evaporation, P the precipitation rate (defined to be positive, even though it represents a downward flux of mass). α, $-\beta$ are the thermal and haline coefficients of expansion. h_B is the e-folding depth for the penetrating component of radiation. The estimate $I(z) = 0.45\,R_s \exp(zh_B)$, with $h_B = 23$ m, provides a good fit to the mean radiative fluxes measured by Siegel et al.(1995) near the IMET mooring, between 10 and 60 m. The observed mixed-layer depth h usually falls in this range in the IMET data set. Niiler and Kraus note that their model results are not very sensitive to the choices of the "constants" m_0, n_0. Chen et al. (1994a) take their values from Davis et al's (1981) analysis of data from the MILE experiment, in winter off Vancouver; they are taken as 0.4, 0.18 respectively. Earlier authors recommended considerably larger values for m_0, but Davis et al. found that the earlier values were estimated from time series of data that were too short.

The physical interpretation of (1) is easier in the form (1'). The first term on the RHS of (1') represents the power of direct wind stirring for deepening the mixed-layer; it is always positive, but is evidently extremely small at small wind speed. B_0 is the flux of buoyancy that is trapped strictly at the surface, so the second term hB_0 describes the rate of potential energy inserted into the layer by the surface buoyancy effects. It is positive except during heavy rain, or on light-wind, sunny days, when the non-penetrating component of shortwave radiation can exceed the sum of longwave radiation, latent and sensible heat losses for several hours.

Because $n_0 = 0.18$, the third term of (1), namely $[-(1-n_0)h_K(|B_0|+B_0)/2]$ nearly cancels the second term whenever B_0 is positive (i.e. whenever convective overturn is occurring). When convection is not occurring, the third term of (1') is zero. It is a dissipative term. The last term of (1') describes the rate of change of mixed-layer turbulent kinetic energy due to the penetrating radiation; it is always negative during the day, and zero at night.

When the RHS of (1) turns negative after a period of being positive, it is assumed that turbulence will die away at the bottom of the mixed-layer, i.e. "detrainment" occurs. In the Niiler-Kraus and Chen et al. schemes, the mixed-layer depth h_K is then calculated by finding the depth for which the RHS of (1) is zero.

In the Power et al. version, the number of model layers fully within the mixed-layer is then found; within these layers, the eddy viscosity and diffusivity are set to a large value ν_m. We have taken $\nu_m = 3\times10^{-3}$ m^2 s^{-1} (its value puts an upper limit on the possible time step through a well-known numerical instability condition). For the model layer containing the mixed-layer interface, the eddy diffusivity is reduced in proportion to the fraction of the model layer occupied by the mixed-layer.

Finally—and crucially, for incorporating the Price et al. mixed-layer mechanism—Chen et al. (1994a) assume that below the mixed-layer, the eddy diffusivity and viscosity are strong functions of Richardson number, as described by Pacanowski and Philander (1981), i.e.:

$$\nu_R = \nu_m(1+5*\mathrm{Ri})^{-2} + \nu_b$$
$$\kappa_R = \nu_m(1+5*\mathrm{Ri})^{-3} + \kappa_b \qquad (3)$$

Our maximum eddy diffusivity ν_m is somewhat lower than the value of 5×10^{-3} m^2 s^{-1} recommended by Pacanowski and Philander (1981). In (3), Ri is the gradient Richardson number:

$$Ri = (g/\rho)(\partial\rho/\partial z)/(\partial u/\partial z)^2 \qquad (4)$$

The background values ν_b, κ_b used in (3) were 10^{-4}, 10^{-5} m^2 s^{-1} respectively. We have also performed a few experiments, described below, with ν_R, κ_R replaced by the observationally based formulae of Peters et al. (1988); this made no significant difference to the results (in the one-dimensional model studies reported here).

To get a feel for how the model works, consider the solution of (1) in mid-morning. Under these conditions of increasing insolation and decreasing mixed-layer depth, the RHS of (1') will be negative at each time step, so the depth h_K will be found by setting the RHS of (1') to zero. Furthermore the third term on the right of (1') is zero. In turbid conditions ($h_B = 0$) the solution is:

$$h_K = 2m_0\, u^{*3}/|B_0 + J_0| \qquad (5)$$

with $m_0 = 0.4|B_0 + J_0|$ is the net buoyancy flux into the water; it will increase through a sunny morning, so h_K will decrease. For a typical Trade Wind speed U of 5 m s^{-1}, $u^* = (C_D\rho_a/\rho)^{1/2}\, U = 0.007$ m s^{-1}, while for a mid-morning net heat flux Q of -300 w/m^2, $|B_0 + J_0| = (\alpha g/\rho C_p)Q = 1.8*10^{-7}$ $m^2 s^{-3}$, leading to h_K = 4m. For U = 1 m s^{-1}, this reduces to 0.032 m. Such estimates of h_K are somewhat deeper in transparent water. With such thin mixed layers, the momentum induced by the (small) wind stress is then deposited into the (extremely thin) mixed-layer, and strong shears develop across its base; the Richardson number mixing then comes into play, and layers with finite stratification and Ri close to 1/4 develop near the surface.

In the afternoon and night, the RHS of (1) is usually positive, and the Kraus depth therefore deepens according to (1). The mixed-layer depth is reset the next morning.

4. NUMERICAL IMPLEMENTATION AND TIMESTEPPING PROCEDURE

To implement (and test) this scheme in the context of the MOM code, a small model domain was defined with a 3 x 3 horizontal array of (T,S, ρ) points, with a 3 x 3 array of (u,v) points embedded around it in the usual MOM configuration (Fig. 1). (T, S, ρ) are defined at all exterior points to be equal to those at the central point, while velocities at each horizontal point are equal (though not necessarily zero). This model domain ensures one-dimensional behaviour within the full MOM architecture—horizontal gradients of temperature and flow divergence are zero, so both vertical and horizontal advection are also zero.

At each timestep pair, the eddy viscosity and diffusivity are estimated at each level, using (1)-(4) above, and the effects of viscosity and diffusion over two time steps are estimated. The surface fluxes of momentum, heat and salt are applied as surface boundary conditions in this calculation. Note that it is the *surface* flux of heat that is applied. The penetrating radiation

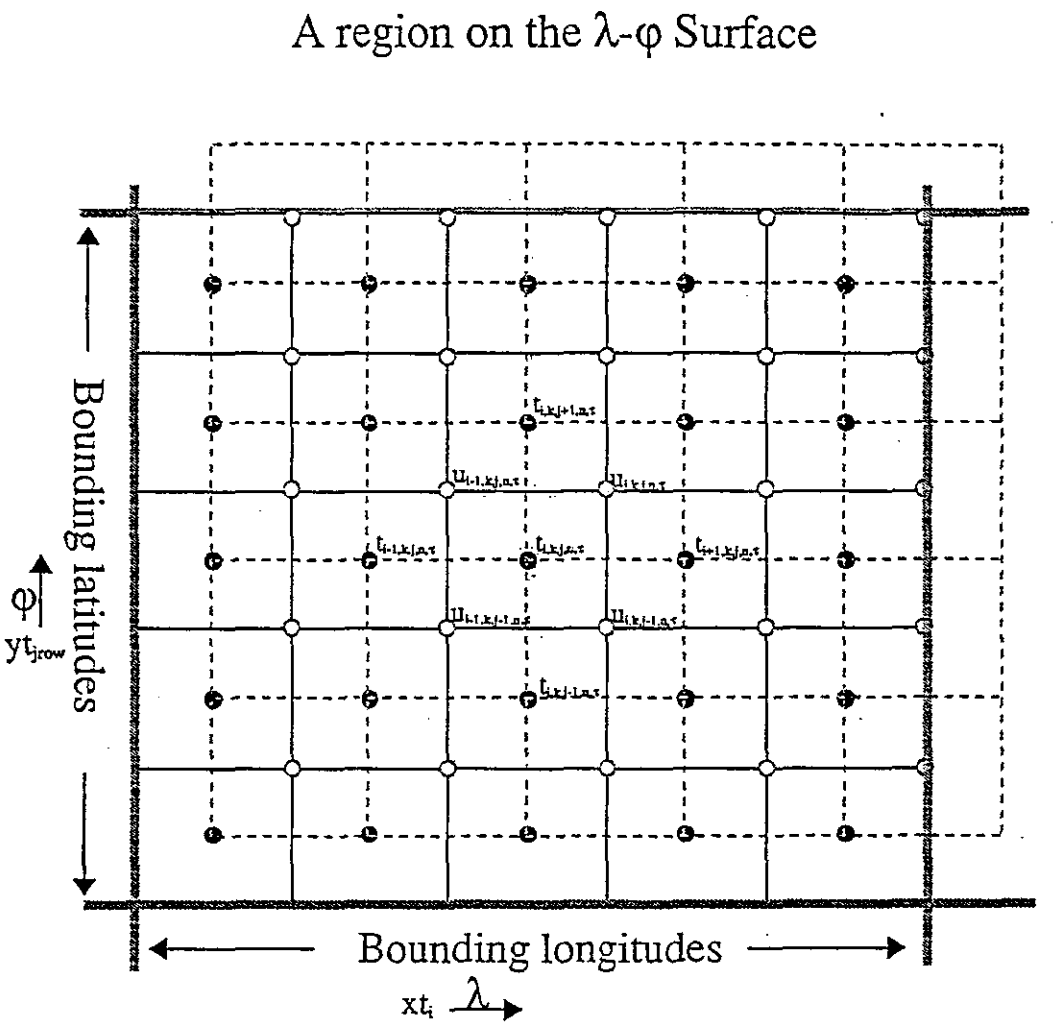

Figure 1: Grid arrangement within the modified MOM model, for the 1-D simulations reported here. •: (T.S.) points; 0: (u,v) points. From Pacanowski (1995).

(taken as 45% of the net shortwave radiation) is distributed according to a transparency profile, and the resulting warming over two time steps directly added at each level according to:

$$T(t+\Delta t) = T(t-\Delta t) + 2\Delta t\,[\partial / \partial z(F_{diff} + F_s)] \qquad (6)$$

where F_{diff} and F_s are the vertical heat fluxes due to diffusion and shortwave radiation, respectively. (The use of two time steps rather than one is needed for MOM model stability). The resulting density profile is corrected for any convective instability before the next time step.

The model was first run with a uniform vertical grid of 2 m depth; then with a coarser grid with the top eight levels having 15 m depth each, increasing below that as in Table 1. The second grid is more representative of the kind of grid that must be used in a full coupled model, due to computer limitations.

5. OBSERVED FLUXES AND INITIAL CONDITIONS FOR THE COARE TEST

The basic data (Weller and Anderson, 1996) consist of standard meteorological observations of air temperature and humidity, wind speed and direction, long and shortwave incoming radiation and SST, made at a moored buoy (the "IMET" buoy). These data and the fluxes estimated from them have been subjected to such exhaustive testing against nearby standards (including eddy-correlation measurements of fluxes) that we are confident of their accuracy to about 10 W/m^2 (for flux validation procedures, see Godfrey et al., 1997). Furthermore, data are available for directly estimating horizontal and vertical advection (Huyer et al. 1993, 1994; O'Malley et al. 1994). While these data are not used here, the indications are that horizontal advection rarely contributes as much as 10 W/m^2 to the net heat budget of the surface mixed-layer (Anderson et al. 1996).

Figure 2, from Weller and Anderson (1996), shows the observations of the daily-averaged net heat flux into the water; it also shows two-hourly averages of the components of wind stress, and of the net heat flux and its four components. Readers are referred to Weller and Anderson for a detailed discussion of these fluxes. Figure 3 shows the cumulative time integral of (P-E). The precipitation estimates were obtained from optical rain gauges on the IMET mooring and on the nearby "Moana Wave"; they probably overestimate the rainfall by about 15% during strong winds, but the model's SST does not turn out to be very sensitive to salinity (Weller et al., 1996). Figure 4 shows the observed initial profiles of temperature and salinity. These were interpolated onto the model's vertical grid. The initial velocity was taken to be zero, at all depths; this may have resulted in some transient mixing events (or their lack) in the first several days of the simulation.

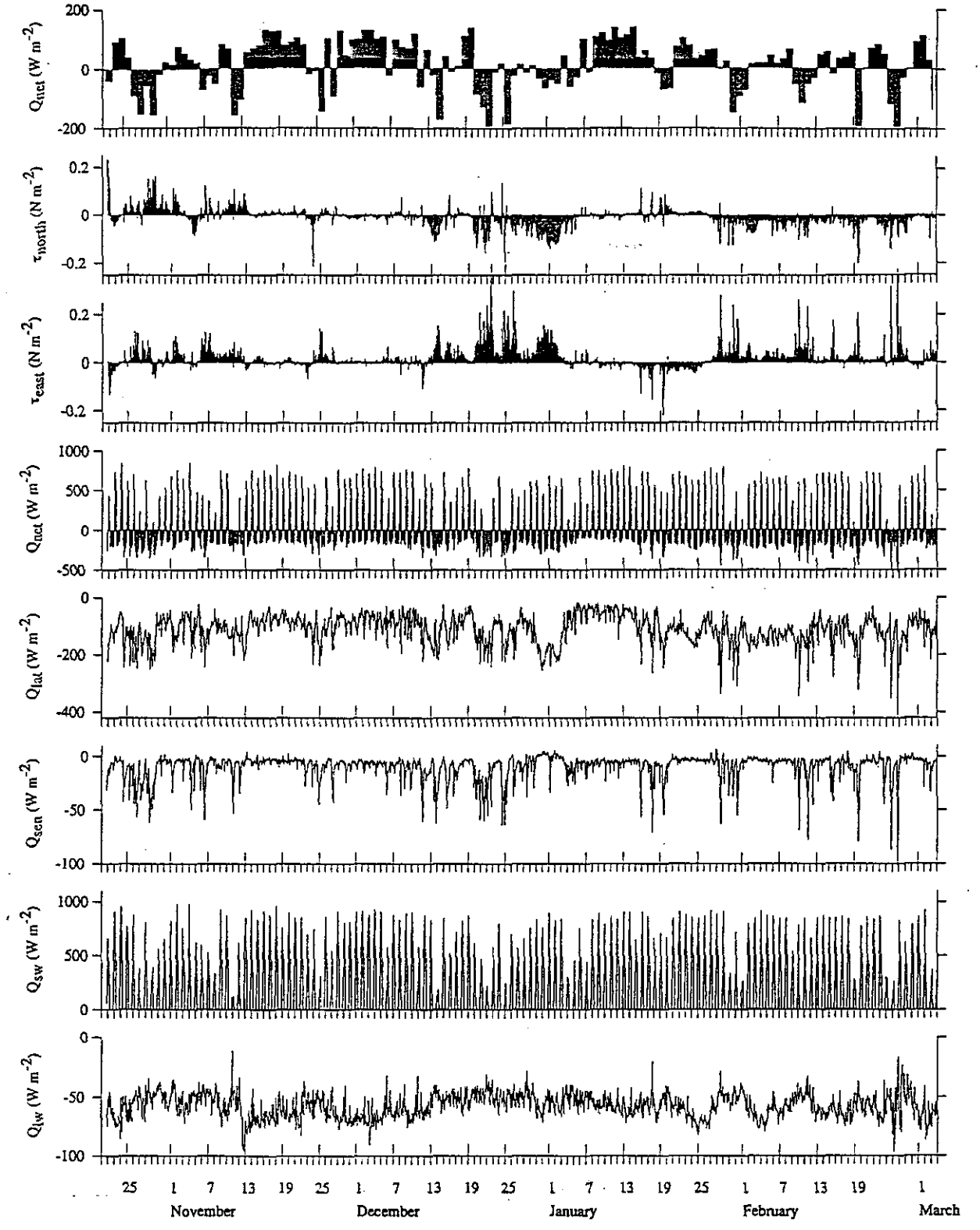

Figure 2: Time series of observed surface fluxes at the Woods Hole Oceanographic Institution IMET buoy, November 1992 – February 1993. From top to bottom, daily-averaged net heat flux; two-hourly averaged wind stress components, towards the north, and the east; net heat flux; and its four components (latent, sensible, shortwave and longwave radiation) (from Weller and Anderson, Figure 6).

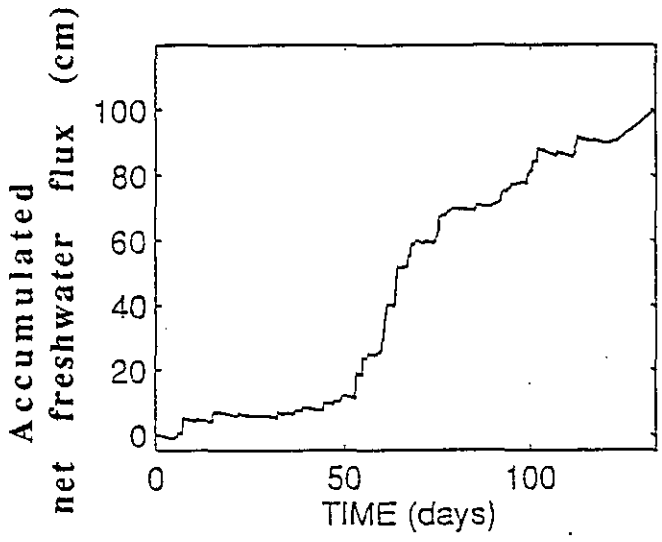

Figure 3: The cumulative time integral of the net (precipitation-evaporation) or (P-E).

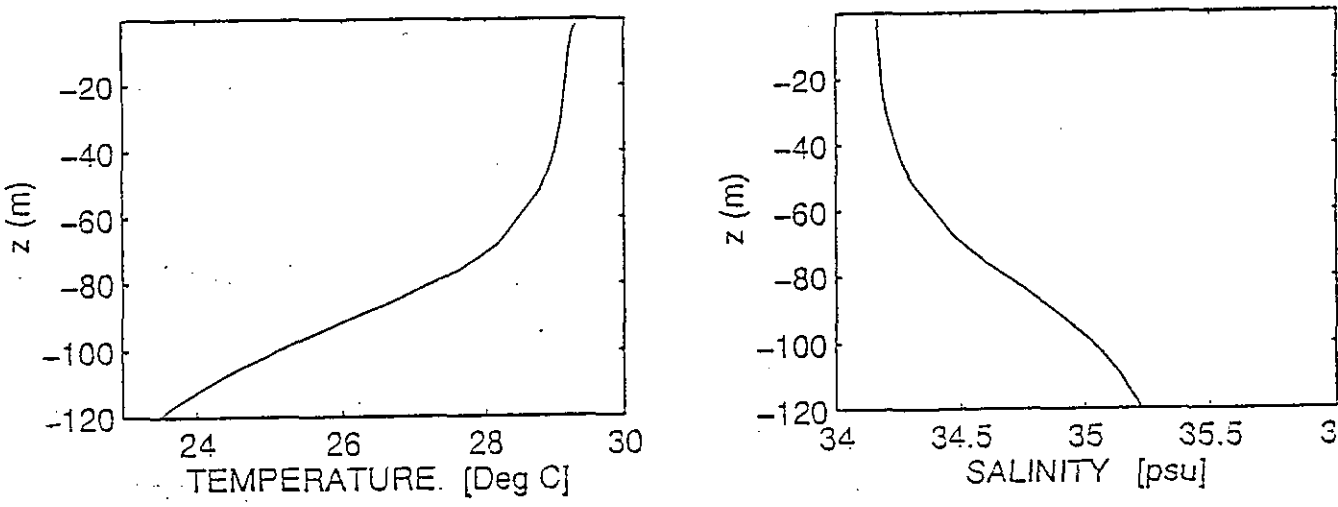

Figure 4: The initial profiles of (a) temperature and (b) salinity at the IMET buoy.

6. RESULTS OF TESTS OF MIXED-LAYER MODELS

6.1 Tests of Chen-Power scheme and modified Price scheme

The lower panel of Figure 5 shows the observed SST at 1.1 m depth, at the IMET buoy location. The upper panel shows the results from the top level of the "fine-grid" (2m resolution) model run; it may be thought of as the model's estimate of mean temperature in the top 2 m. By comparison, Figure 6 shows the observed SST again, and the result of running the Price et al. model over the same period, from Weller and Anderson (1996). The light lines in Figs. 6a,b show temperature at 9 m depth.

As discussed in Weller and Anderson (1996), the Price et al. model underestimates the observed decrease in SST in late October, and also the decrease in late December-early January. These two discrepancies can be seen in Figure 6. Anderson et al. (1996) ascribe the first fall to strong horizontal advection at that time (in agreement with Cronin and McPhaden's (1996) observations at (0°,156°E), 200 km away). Anderson et al. (1996) suggest that the second temperature decrease may be due to an underestimation by the Price et al. model of mixing and turbulent heat fluxes into the stratified water below the mixed-layer, during the westerly wind burst that occurred during this time.

It is therefore interesting that the Chen-Power scheme displays very similar discrepancies. This is to be expected on the first occasion, (days 1-7), where the problem is thought to be due to horizontal advection (not included in either scheme); but it is somewhat surprising in the prolonged strong winds of the second occasion (days 44-74), where it was expected that the Chen et al. scheme would lead to deeper mixing. Since writing this, Feng et al. ( ) have shown that northward advection during this westerly wind burst accounts quite accurately for the discrepancy. The Chen-Power scheme also underestimates the amplitude of the diurnal cycle somewhat, on calm days; this is believed to be because the 2 m resolution of this version of the scheme is still rather coarser than the observed depth scale of temperature variations on calm days (by contrast, Weller and Anderson (1996) used a 0.25 m depth scale).

To further test the performance of the Chen-Power scheme during the westerly burst, we first obtained the Kraus depth, h_K, for the run with this scheme (Fig. 7b). It is consistently less than the density-based mixed-layer depth h_σ, from a run with a grid interval of 2 m and a density difference (in σ_t) from the surface of 0.01, (Fig. 7a)—even during the prolonged westerly wind burst of days 44-74. This suggests that Richardson-number dependent mixing may be the prime mixing influence in the Chen-Power scheme at all times in this simulation. Furthermore, the simulated h_σ matches observations remarkably well. Figure 8a shows the data of Figure 7a, displayed in a format for easy comparison with equivalent observational data (Fig. 8b, bottom of shaded portion) from Anderson et al. (1996). Figure 8c, from Anderson et al. (1996), shows h_σ simulated with the original Price et al. (1986) model. The two simulations of Figs. 8a and 8c are quantitatively very similar, even during the westerly wind burst period (days 44-74) when SST decreases more rapidly in the observations than in the model. This was also true of the simulated h_σ from our modified Price scheme (not shown). All three simulations match the observed h_σ of Figure 8b quite well.

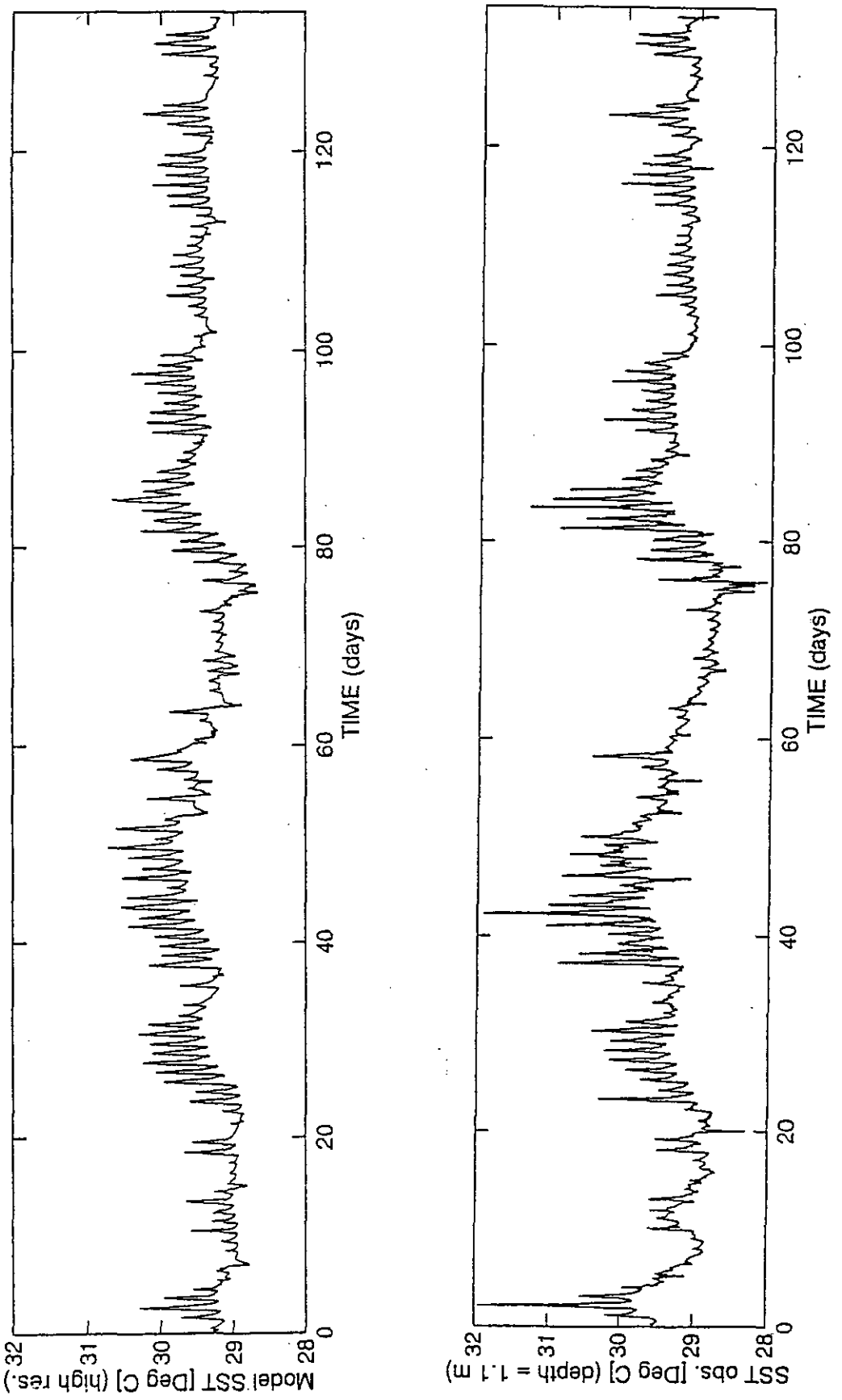

Figure 5: Upper panel: temperature from the top level of the "fine-grid" (2 m resolution) run with the Chen-Power scheme. Lower panel: observed SST at 1.1 m depth at the IMET buoy site.

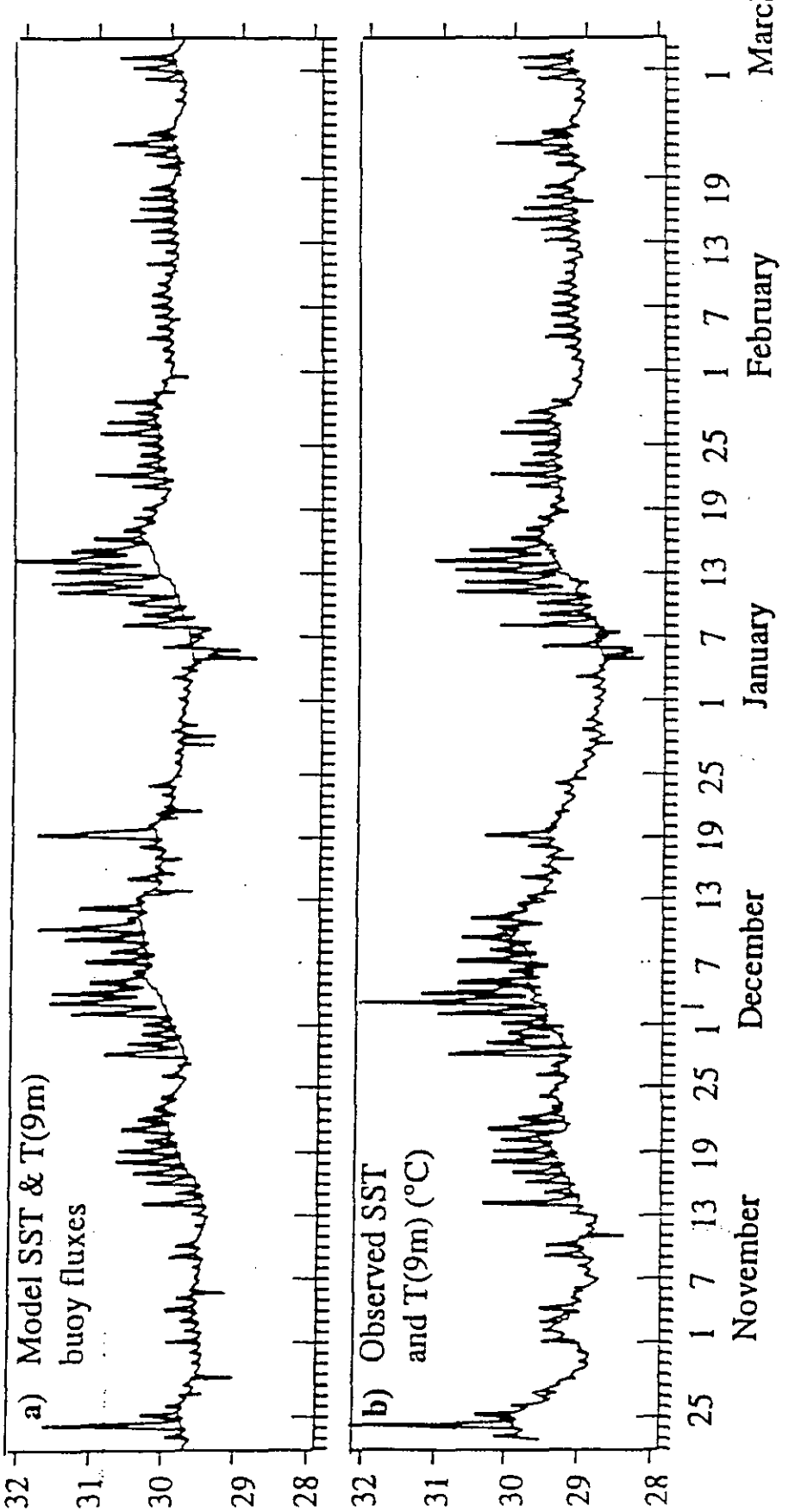

Figure 6: Upper panel: temperature from the top level of a simulation with the full Price scheme, with a grid interval of 0.25 m. Lower panel: observed SST at 1.1 m depth, at the IMET buoy location. From Weller and Anderson (1996).

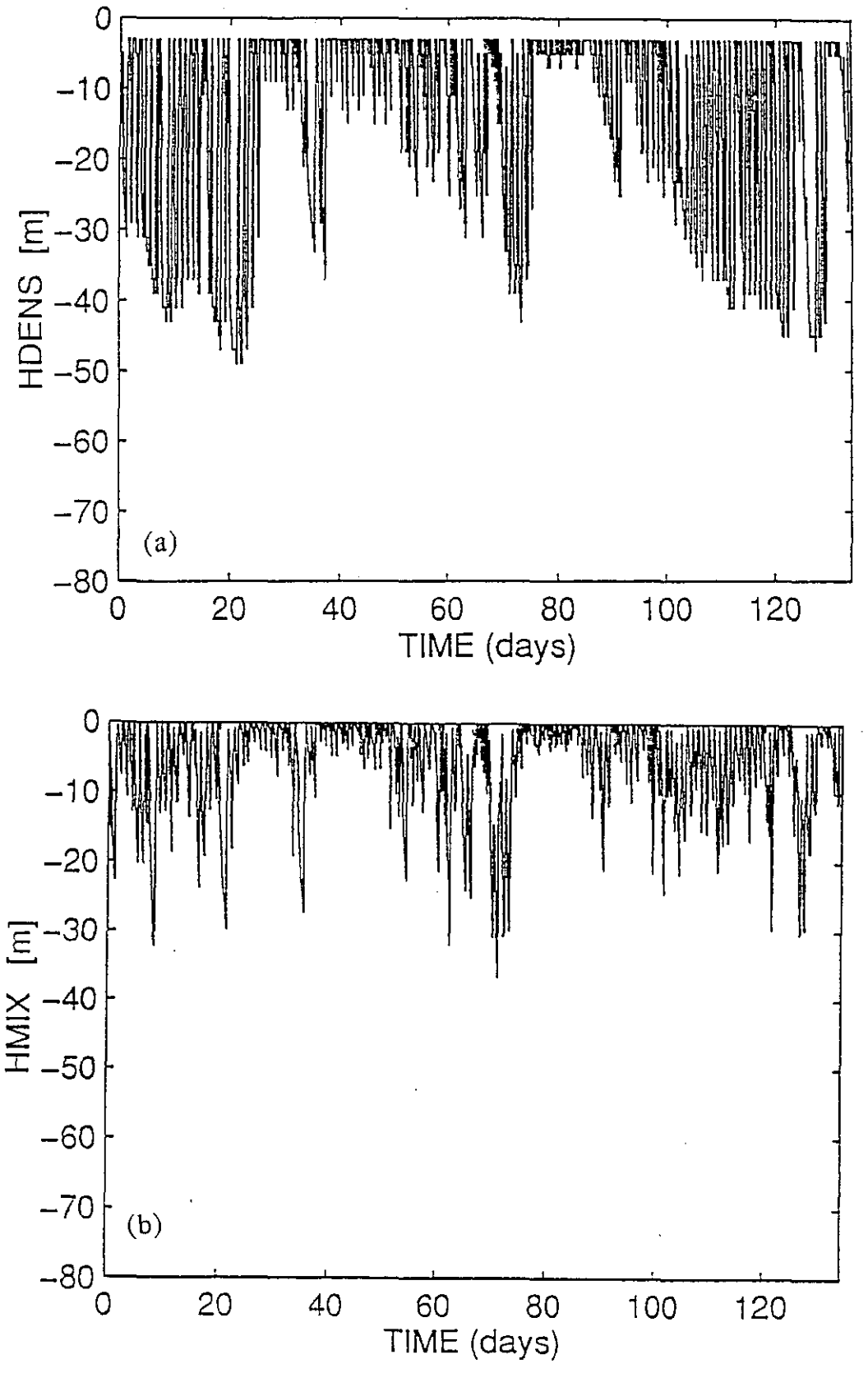

Figure 7: (a) Density-based mixed-layer depth h_σ (for a σ_t difference of 0.01 across the layer) from the Chen-Power run. (b) Kraus depth for the Chen-Power run.

As a further check that the Niiler-Kraus mechanism plays no significant role in setting mixed-layer depths and SSTs when the modified Chen scheme is run for the IMET data, we created a "modified Price scheme" by setting the Niiler-Kraus depth h_K to zero at every time step. Figure 9 shows observed SSTs again, and those modeled with the modified Price scheme. The simulated SSTs are very similar to those of Figure 5. This result is seen more clearly by comparing Figure 10a, which shows (Observed SST-Modelled SST) for the Chen-Power scheme, with Figure 10b, which shows the same quantity for the modified Price scheme. The differences are almost identical, except for a few days near day 50. Density-based mixed-layer depths h_σ from the modified Price scheme (not shown) are also almost identical to those from the Chen et al. (1994a) scheme, Figure 8a.

As previously noted, Feng et al. (1997) found that advection of colder water from the south past the IMET mooring significantly coold SST's during the westerly wind burst of days 44-74. It seems probable that this is the major cause of the failure of the three 1-D models discussed here to simulate SST's correctly during this period. However, it should also be noted that Smyth et al. (1996) show time series of turbulent heat fluxes at the $\sigma_t = 22.0$ isopycnal during COARE (full line, Figure 11). This isopycnal lay well below the mixed-layer during their observations. The turbulent flux across it is near zero most of the time, but it sometimes reaches over 100 W/m^2, in strong spikes. Such phenomena are not accounted for by either the Chen-Power et al. or modified Price et al. model, so the model clearly has deficiencies.

6.2 Dependence on latitude

It was felt that the dominance of Richardson-number dependent mixing illustrated by Figures 7 to 10 may be confined to a fairly narrow band near the equator. In this band, the inertial period is considerably longer than a day, so that momentum inserted in the mixed-layer by steady winds build up large downwind velocities before Coriolis effects rotate these velocities sideways. Consequently, shears from succeeding days build up, and Richardson number mixing may result in greater deepening than would occur at higher latitudes with the same fluxes.

However, our results do not support this idea. Figure 12 shows the model SST, density-based mixed-layer depth and Kraus depth from a run with identical conditions to those of Figures 5 and 7, but at 20°S—ten times higher in latitude than the COARE observation site. Comparison with Figures 5 and 7 shows remarkably small differences. Density-based mixed-layer s are slightly shallower in Figure 12 than in Figure 7. Unfortunately, time has not permitted us to follow up this puzzling result further. However, the result suggests that—if IMET fluxes are qualitatively representative of conditions throughout the Warm Pool-then Richardson number mixing must dominate the mixed-layer formation process throughout the Warm Pool (except, perhaps, in tropical cyclones, when the u^{*3} term in (1) must increase dramatically).

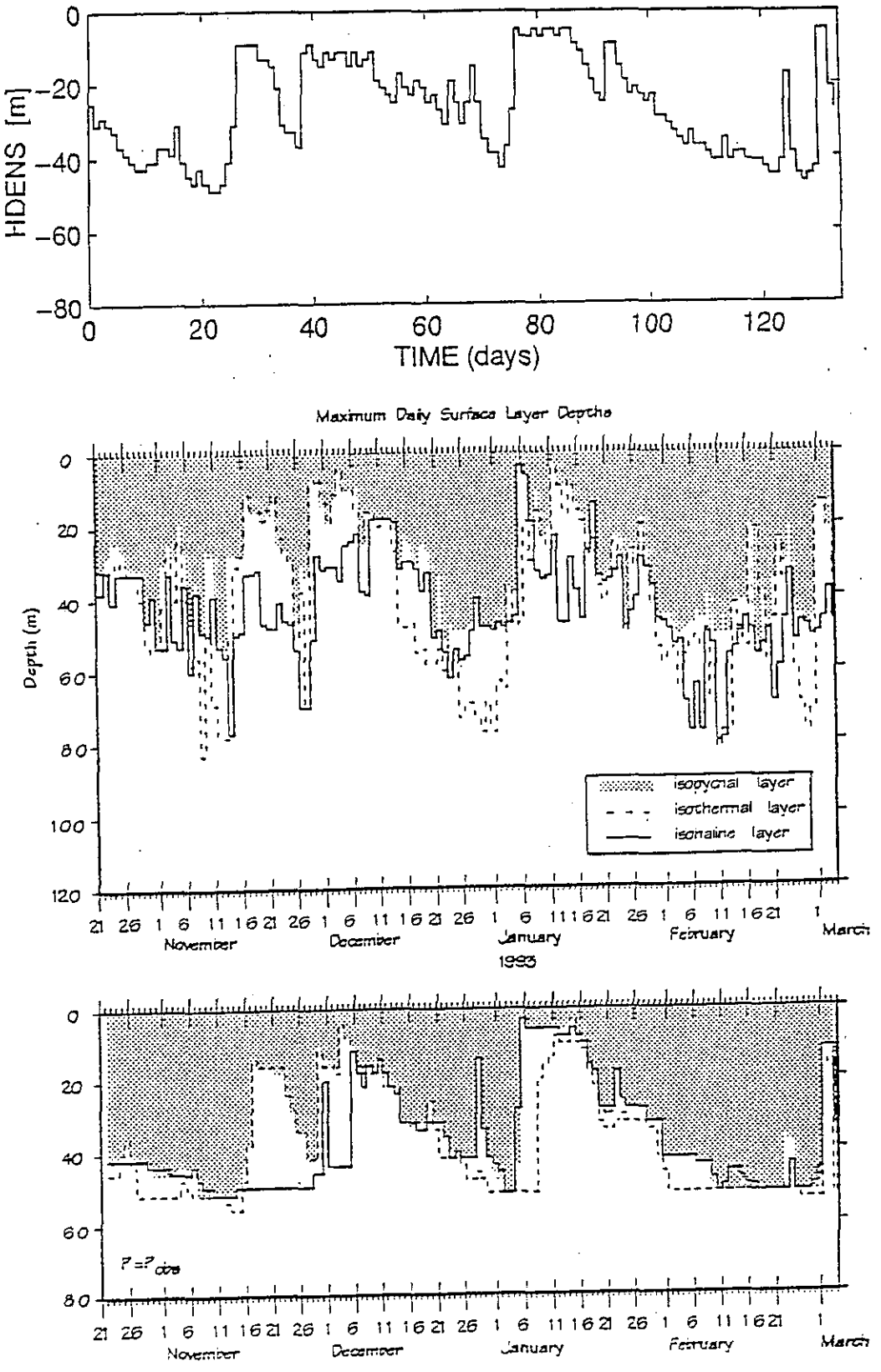

Figure 8: (a) Modelled h_σ, from the Chen-Power simulation, (b) Observed h_σ near the IMET mooring, (c) modelled h_σ, from a Price et al. simulation. The base of the grey shading indicates h_σ. Note different depth scales in (b) and (c). Parts (b), (c) from Anderson et al. (1996).

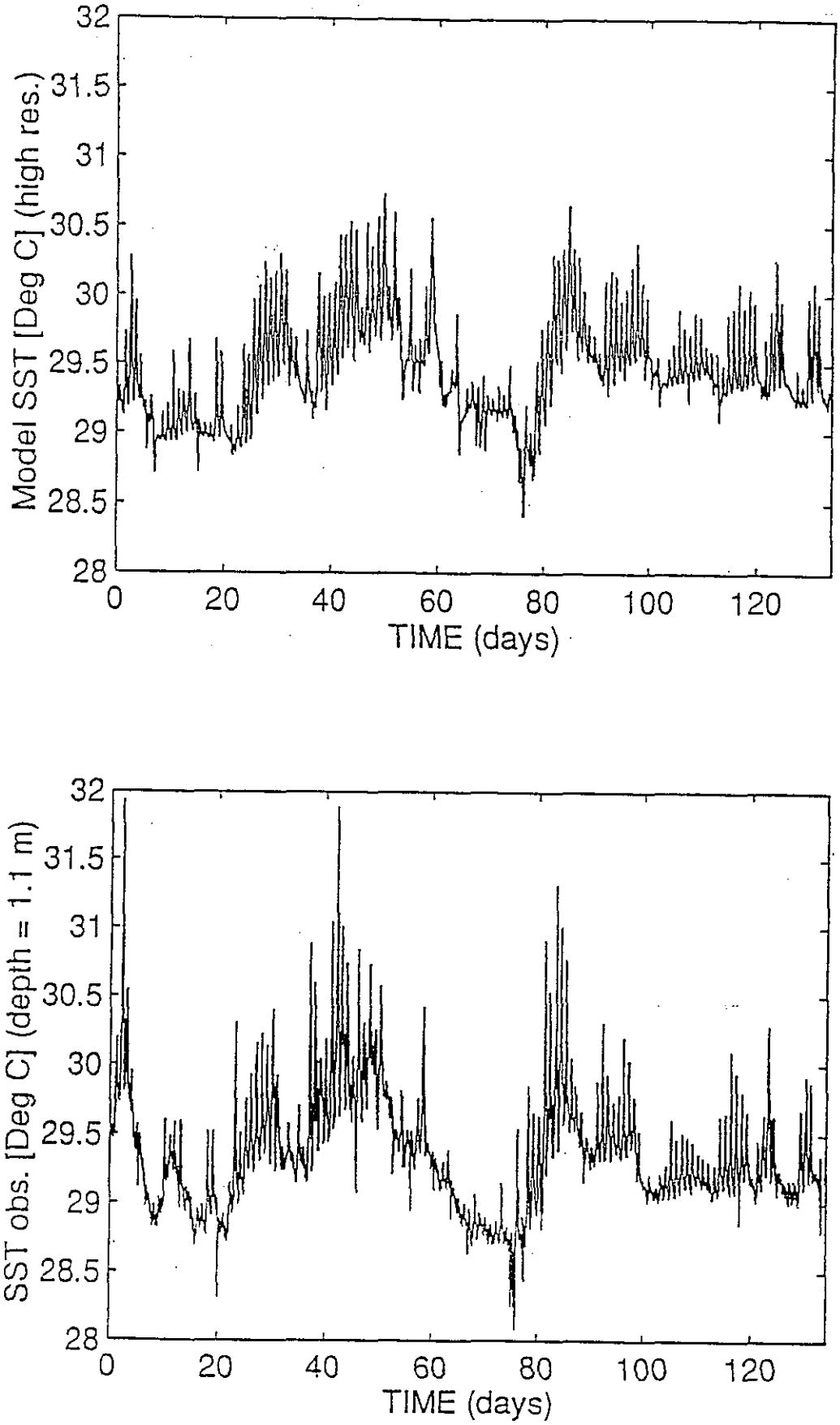

Figure 9: Upper panel: temperature from the top level of the "fine-grid" (2 m resolution) run with the modified Price scheme. Lower panel: observed SST at 1.1 m depth at the IMET buoy site.

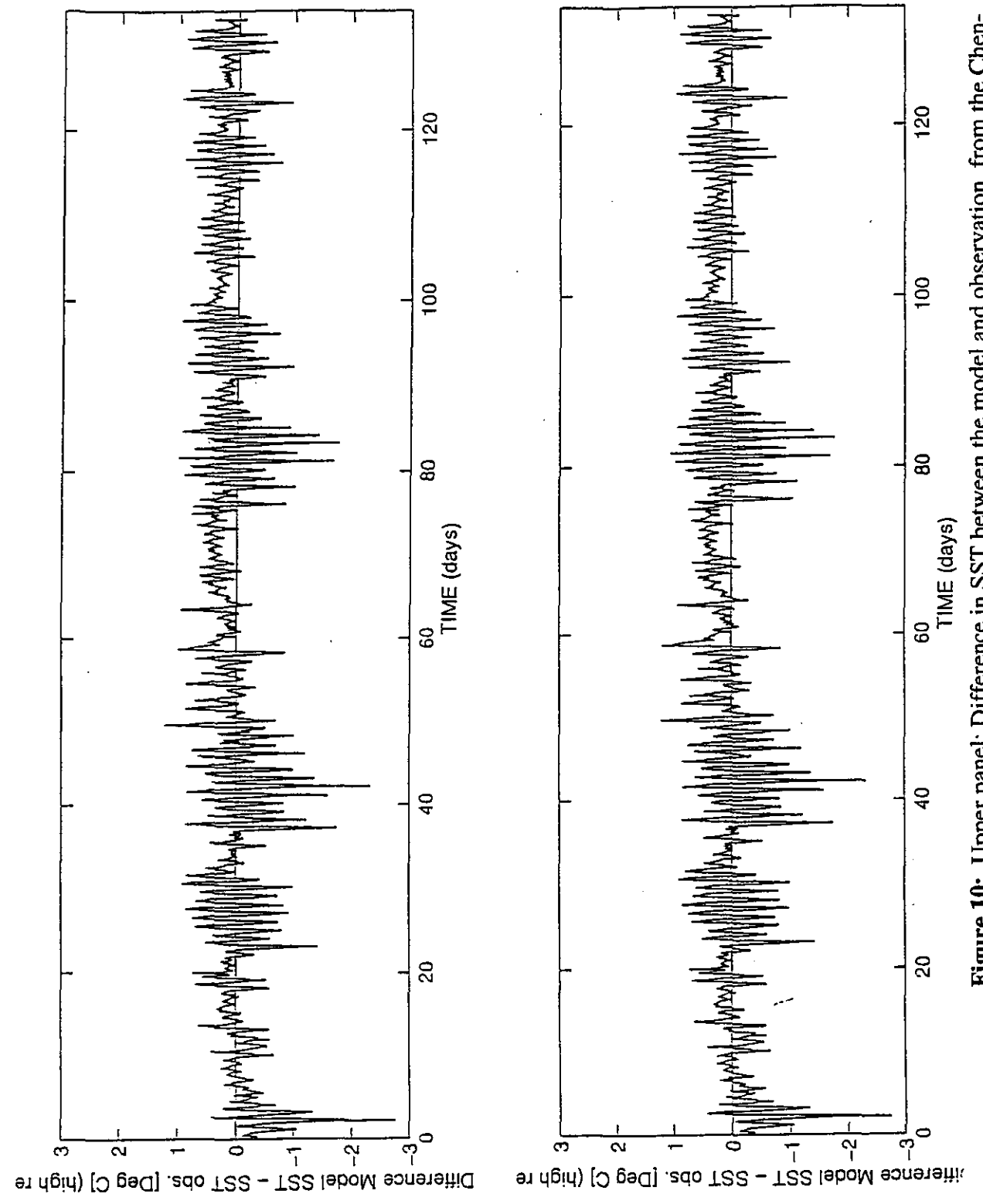

Figure 10: Upper panel: Difference in SST between the model and observation, from the Chen-Power scheme. Lower panel: the same quantity, from the modified Price scheme.

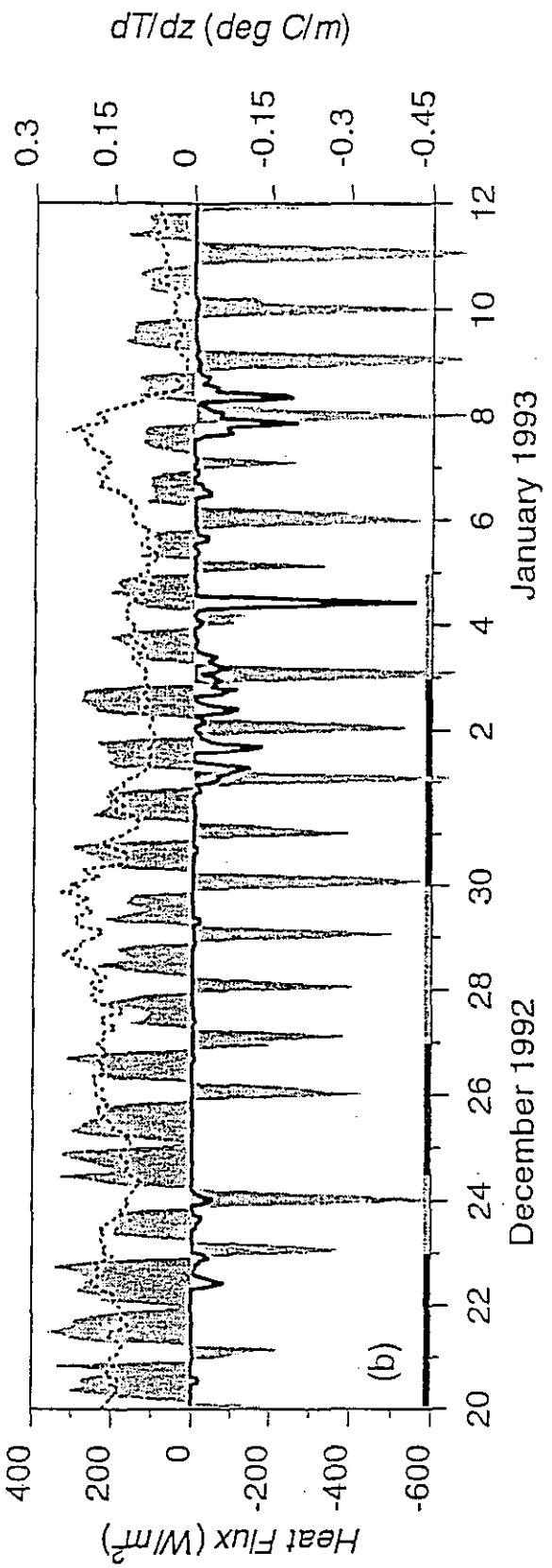

Figure 11: The full line shows measured turbulent heat fluxes through the 22.0 isopycnal, near the IMET mooring. (From Smyth et al. 1996).

6.3 Sensitivity to parameterisation of Richardson-number-dependent mixing

Peters, Gregg and Toole (1988; referred to as PGT below) made direct measurements of eddy diffusivities near the equator; S. Wilson (pers. comm.) fitted their data with an analytic expression similar to (4), but with a sharper drop-off of diffusivities with increasing Ri than those of Pacanowski and Philander (1981; referred to as PP). Experiments similar to those discussed in 6.1 above showed almost no difference. We also experimented on the equator, with both (4) and the PGT equivalent; once again, we found differences of less than 0.1°C.

However, it should be noted that the full 3-D OGCM is sensitive to changing from the PP to the PGT scheme, at least along the equator. The 3-D circulation in this region is an extremely complex system, dependent on horizontal and vertical advection which in turn depend on diffusively determined currents, so it is not surprising that the 3-D system should display this sensitivity when the 1-D system does not.

6.4 Sensitivity to flux errors

A major motivation for the COARE experiment was that heat flux accuracies of order 10 W/m^2 were believed to be needed if the SST changes of order 0.5°C that precede ENSO events were to be predicted in coupled models. This accuracy appears to have been achieved in COARE. To more rigorously test the sensitivity of SST to changes in heat fluxes of this order, we here investigate the effect of a steady increase of 10 W/m^2 to the IMET fluxes on the predicted SSTs.

Figure 13 shows the difference in SST between the model and observations resulting from this change in the applied heat flux (which is all applied at the surface). As expected, model SST increases fairly rapidly (at least on daily average) compared to observation, for the first 30 days. However, the SST difference appears to equilibrate after this time.

The reason for this behaviour is interesting. Figures 14a,b show the temperature difference and salinity difference, respectively, between the present run, and the original "control" run with the Chen-Power scheme. The mixed-layer depth (not shown) decreases in the enhanced-flux run, relative to the control run. As a result the freshwater input is trapped in the shallower mixed-layer and freshens it faster, while the water below the mixed-layer, deprived of freshwater from the surface, does not freshen as fast (Fig. 14b). The rapid warming near 50 m in the last 60 days (Fig. 14a) is due to penetrating radiation. During this time, the extra heat is absorbed here, rather than at the surface. Because this water is at the same time becoming saltier (relative to the control run), this deep heating does not result in convective overturn.

This mechanism is physically realistic; and it provides a negative feedback mechanism, tending to reduce the change in SST caused by changes in the net surface heat flux. As such, it may be part of the explanation for the very steady SST maximum in the Warm Pool region.

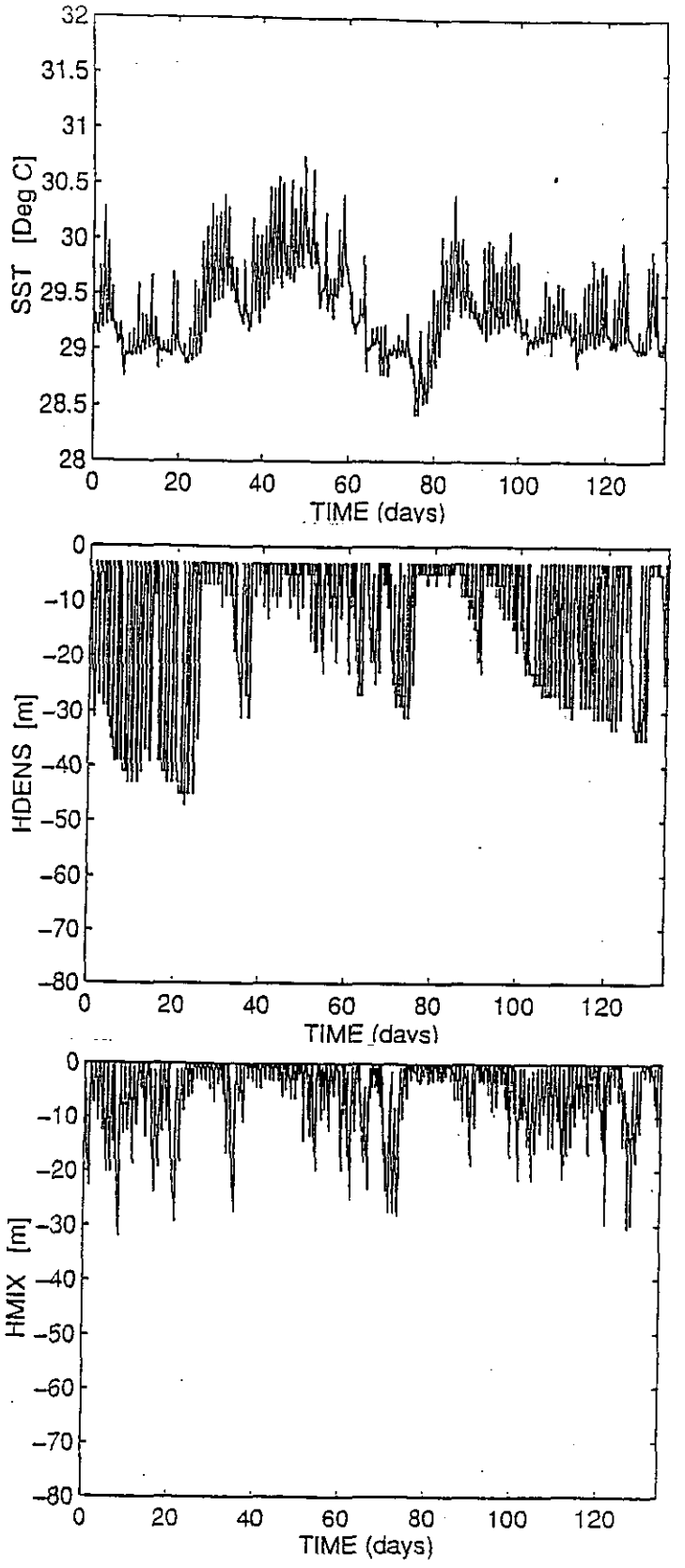

Figure 12: SST, h_σ and Kraus depth for a run of the Chen-Power scheme, but with latitude set to 20°S. Comparison with Figures 5 and 7 shows surprisingly few differences.

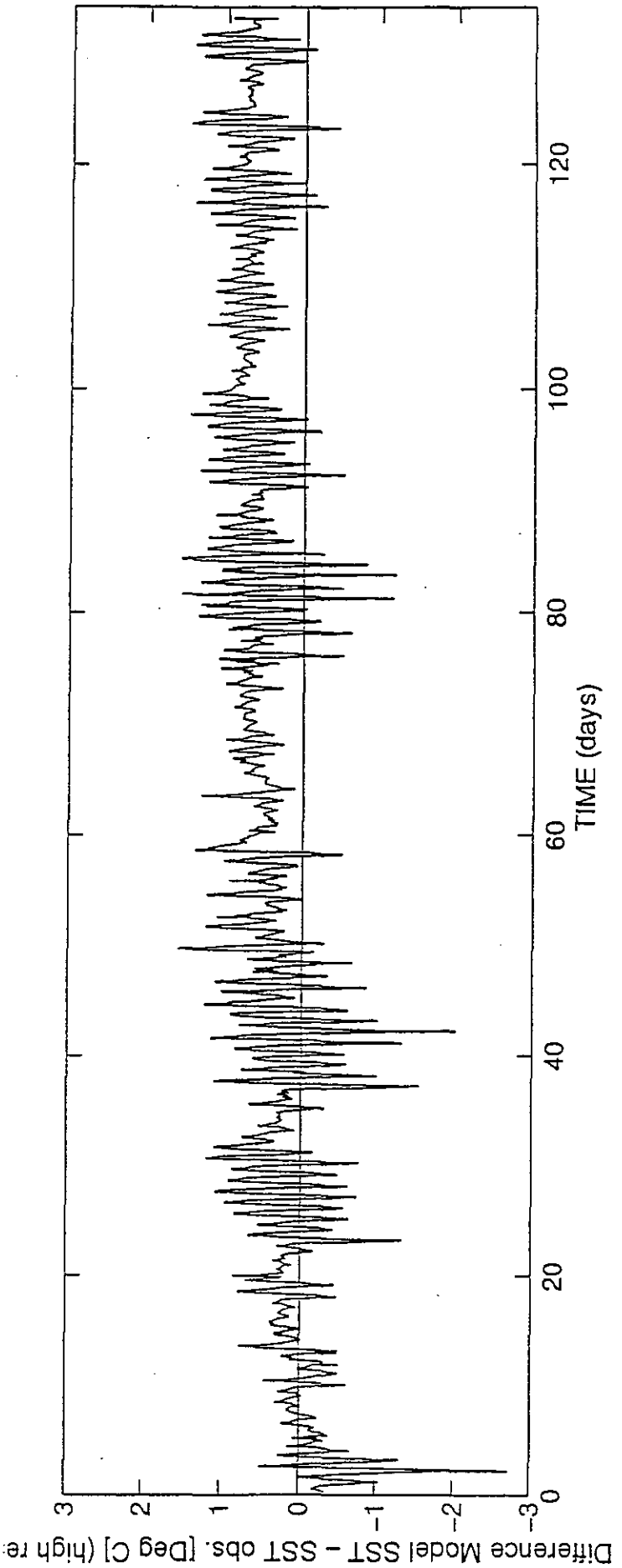

Figure 13: Difference in SST between model and observations, for run of the Chen-Power scheme with 10 W/m^2 added to the applied surface heat flux.

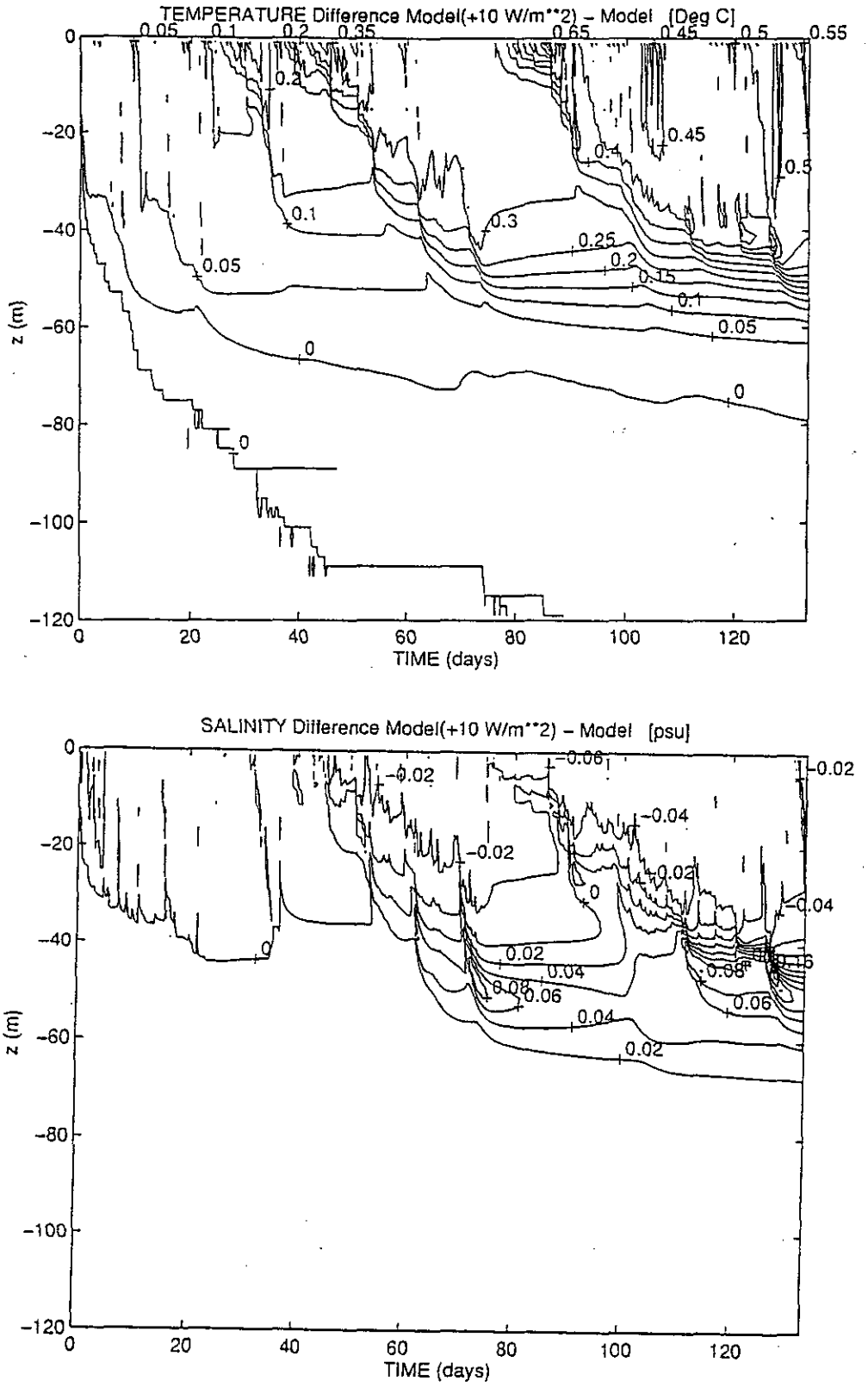

Figure 14: (a) Temperature and (b) salinity differences between the enhanced-flux run and the control run.

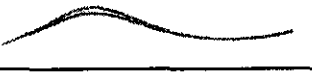

Another point to note is that (model SST- observed SST) is substantially greater in Figure 13 than in Figure 10. This implies that the differences in Figure 10 are just as likely to be due to residual errors in fluxes as to errors in mixed-layer physics.

7. HEAT FLUX FORMULATIONS

In this section we describe our choice of surface heat flux boundary condition for the LWRRDC model, and report some tests of it against the IMET flux data set.

7.1 Literature review

7.1.1 Basics

The total heat flux is given by:

$$Q_{tot} = Q_{surface} + cR_s \tag{7}$$

where, as above, we adopt the convention that *upward* heat fluxes are positive; thus the shortwave radiation R_s is always negative. cR_s is the penetrating fraction of radiation—c is usually taken to be between 0.38 and 0.45, though early authors (and some late ones) used 0.0. The part of the heat flux absorbed at the ocean surface, $Q_{surface}$, is given by:

$$Q_{surface} = E_0 + H_0 + R_1 + (1-c)R_s \tag{8}$$

where E_0, H_0, and R_1 are the latent, sensible and net longwave heat losses (all usually positive). $Q_{surface}$ is positive at night, and for much of the day. A variety of empirical algorithms have been suggested for relating the four terms R_s, E_0, H_0, and R_1 to standard marine meteorological observations. The meteorological observations used are Sea Surface Temperature T_s; air temperature T_a; air specific humidity q_a; wind speed W; and total cloud cover C (though some formulae distinguish between different cloud types). We will ignore the latter possibility; thus for a given choice of empirical formulae we can write

$$Q_{surface} = F(T_s, T_a, q_a, W, C) \tag{9}$$

where F is a specific analytic function of the 5 variables.

One choice for the boundary condition on an OGCM would be to apply observationally-determined fluxes estimated from (9), using observations of T_s, T_a, q_a, W, C to provide a surface heat flux that is a fixed function of time. However, because of consistent errors in the observations and the bulk formulae, this approach leads to the model's SST drifting steadily away from observation. In particular, the global and long-term mean heat flux should be zero; departures from this due to errors in the heat flux must lead to an indefinite linear trend in the ocean heat content.

7.1.2 Physical basis for "strong" and "weak" relaxations

A second choice of OGCM boundary condition (Haney 1971) is to use (9), with T_s replaced by the temperature T_{model} of the model's top layer. Haney suggested that all variables except T_s should be fixed in (9), and Qsurface should be estimated by a Taylor series expansion in T_s:

$$\begin{aligned} Q_{surface}(T_{model}) &= F(T_s, T_a, q_a, W, C)|_{Ts=Tobs} + \partial F/\partial T_s (T_{model} - T_{obs}) \\ &= Q_{surface}(T_{obs}) + \lambda(T_{model} - T_{obs}) \end{aligned} \qquad (10)$$

where T_{obs} is the observed SST, and $Q_{surface}(T_{obs})$ is the observed heat flux. Haney found that in most parts of the world, the derivative $\lambda = \partial F/\partial T_s$ was of order +35 $W/m^2/°C$. In the tropics, λ is well approximated by the term from latent heat,

$$E_0 = \rho_a C_E L_w W[0.98 q_{sat}(T_s) - q_a]:$$
$$\partial F/\partial T_s = \partial E_0/\partial T_s = 0.98 \rho_a C_E L_w W[dq_{sat}(T_s)/dT_s]$$

where $q_{sat}(T)$ is the saturated specific humidity above pure water of temperature T, ρ_a is air density, C_E is the bulk transfer coefficient and L_w is the latent heat of vaporisation. The factor 0.98 allows for salinity effects. Oberhuber (1988) provides global maps of mean seasonal values of $-\partial F/\partial T_s$, for a particular choice of empirical formulae. Recalling the sign convention on $Q_{surface}$, it may be noted that this formula for the surface heat flux results in quite a strong restoring tendency of T_{model} towards T_s. For a mixed-layer of depth H, this term alone will lead to T_{model} obeying:

$$\rho C_p H \partial T_{model}/\partial t = -\lambda(T_{model} - T_{obs}) \qquad (11)$$

implying exponential decay towards T_{obs} with a decay time τ of $\rho C_p H/\lambda$. For a typical mixed-layer depth of 50m, τ is about 60 days. We refer to the Haney heat flux boundary condition (10) as providing a "strong" relaxation of model SST towards observations.

Seager et al. (1988) proposed a variant on the Haney (1971) technique. They noted that, in practice, air temperature and humidity are not independent of T_s. In the tropics more than a few hundred km from land, one typically finds that the Relative Humidity $RH = q_a/q_{sat}(T_a)$ is very close to 0.8 (e. g. Kleeman and Power 1995), while $T_s - T_a$ is typically in the range 0.5-1.5°C. Thus T_a—and through RH, q_a—should be treated as functions of T_s. They took $q_a = \delta q_{sat}(T_s)$, with δ a constant, so that their formula for Q_{tot} could be written:

$$Q_{tot} = R_s + \rho_a C_E L_w W(0.98 - \delta) q_{sat}(T_s) + \alpha(T_s - T^*) \qquad (12)$$

The term $\alpha(T_s - T^*)$ in (12) accounts for sensible and longwave heat flux components; T* is chosen so that when $T_s = T_{obs}$, $\alpha(T_s - T^*)$ has the climatological value of the sensible and longwave heat fluxes. α is about 1.5 $W/m^2/C$. The main term in $\partial Q_{tot}/\partial T_s = \lambda'$ then still comes from the latent heat term i.e. $\lambda' \approx \rho_a C_E L_w W(0.98 - \delta)\partial T_s = \lambda'$. This is typically 13 $W/m^2/°C$, which is smaller than λ above by a factor $(0.98 - \delta)/0.98$, which is about 0.3. With λ replaced by λ' in (11), the new decay time $\rho C_p H/\lambda'$ is still dominated by the latent heat term, thus $\rho C_p H/\lambda'$ is about 200 days. We refer to the Seager heat flux boundary condition (12) as providing a "weak" relaxation of model SST towards observations.

Seager et al. note that the use of such a small value of λ' has—apart from the greater realism of its physical basis—real advantages in modelling SST on seasonal or longer timescales, in the

tropical east Pacific. If a "Haney" value of λ is used, cold water upwelled in the eastern equatorial Pacific returns to the "observed" (seasonal mean) SST within about $\rho C_p H / \lambda = 60$ days after upwelling. Ekman transport carries the newly upwelled water only a few hundred km from the equator in this time, so any interannual SST anomalies will only be this wide in such a model. If, however, the weaker constant λ' is used, SST will equilibrate about three times more slowly, and the band of anomalous SSTs will be about 1000 km wide—roughly as observed.

Similar considerations apply to the water upwelled in the northern Indian Ocean in northern summer, which appear from the mean seasonal cycle of heat flux to move up to 1000 km offshore before equilibrating, after upwelling (Godfrey et al. 1995). This suggests that, in testing the ability of an OGCM to generate observed SST anomalies, a weak "Seager" value of relaxation constant should be used. A further reason for adopting the weak value λ' is that, in the coupled model, air temperature and humidity should be related to SST roughly as found by Seager et al. (1988), so tests of the model with the boundary condition (11') will provide a more realistic assessment of the OGCM's performance in the coupled mode than a run with a boundary condition like (11). However, use of a weak relaxation constant means that with typical flux errors of tens of W/m^2, the model can generate SST anomalies of several degrees. Recent modelling results (Chen et al. 1994b) suggest how to deal with this problem.

7.1.3 Recent variations on the choice of boundary conditions

(i) Kleeman and Power (1995; referred to below as KP) developed a quite different model of surface heat flux, based around a prognostic global model of air temperature in the Marine Atmospheric Boundary Layer (MABL). The paper contains some very valuable physical discussion, particularly of why RH is so close to 0.8—basically because the MABL is of nearly constant depth of 500 m and is cloud-topped, so air is saturated at 500 m. The lapse rate applied over 500 m implies a relative humidity of about 80%. (They do not explain, however, why the MABL depth is so constant over the ocean).

KP show a map of annual mean observed RH. It is remarkably constant worldwide: its standard deviation from 0.80 is 0.01-0.02. However, they suggest that the Seager et al. approximation $T_s - T_a$ = constant is *not* very good. KP instead obtain T_a by solving a 2-D equation for it. In this equation horizontal advection (by climatological 850-mb winds) is balanced by horizontal diffusion, sensible heat convergence over the bottom 1000 m, and an estimate of net cooling by longwave radiation.

Using empirical formulae similar to those discussed earlier, and using climatological (COADS) clouds to estimate shortwave radiation, KP estimate an annual mean surface heat flux. It is quite similar to that of Oberhuber (1988). Of particular interest is their examination of the way the surface heat flux responds in their model to a typical east Pacific SST anomaly, with a central maximum of 4°C (Fig. 15a). The corresponding net heat flux anomaly from their model (Fig. 15b) has a similar shape (though note the side lobes to north and south). From its amplitude of 75 W/m^2, we infer a sensitivity λ' of 18.75 $W/m^2/°C$—slightly larger than the Seager value of 10-15 $W/m^2/°C$ (see earlier). Kleeman and Power note a scale-dependency of λ', with larger values at smaller space scales (basically, air advecting across a front in SST will at first absorb heat at a greater rate—higher λ'—before the air mass can equilibrate). For SST patches like those of Figure 15a but with different Gaussian meridional e-folding scales Y, they found that λ' increased from 13 to 27 $W/m^2/°C$ as Y decreased from 15° to 2°. However, the

maximum air temperature anomaly (Fig. 15c) corresponding to Figures 15a and b is only 1.6°C, implying that the anomaly in $(T_s - T_a)$ reaches 2.4°C. This seems unrealistically large, (e.g. Weare et al. 1981, Fig. 12). Lower values of the anomaly in $(T_s - T_a)$ would imply values closer to those of Seager et al.

The KP model offers a possible solution to some rather serious problems that arise in extending the Seager-type approach to higher latitudes. We considered using it, but did not adopt it because of the time involved in adapting their MABL model to our situation. The above results suggest that for the large-scale SST anomalies of interest here we should increase the flux sensitivity λ' from the Seager value (about 10-15 $W/m^2/°C$) to perhaps 15-20 $W/m^2/°C$.

(ii) Another, very different, approach to the problem of parameterising surface heating is that of Ji et al. (1995). At each basic one-week time interval of their ocean model, Ji et al. first advance their model by a week, with *zero* surface heat flux, to obtain a "first guess" SST field. They then simply set the temperature of the top layer of their model (50 m deep) to a linear combination of the weekly observed SST, from Reynolds and Smith (1994), and the first-guess SST. They infer net surface heat fluxes from the result.

This simple approach is attractive (though modifications of it are desirable, such as using a climatological mean $\partial(SST)/\partial t$ at each point to advance the SST at each point, rather than an incorrectly forced model estimate of $\partial(SST)/\partial t$). However, their method has the drawback that all the SST data have been used in forcing the model. There is therefore no direct information on SST anomalies. In principle one could compare the model's anomalies of the net heat flux into the water with those obtained from meteorological means, but it would be hard to interpret these in terms of SST anomalies.

Coupled modellers (and we) need to know how well our ocean model can simulate the observed SST anomalies when it is forced by an observationally based surface heat flux product, taking account of the response of the MABL temperature and humidity to SST. We also need to know the physical mechanisms causing SST anomalies, particularly in the Indian Ocean where the physics of SST change is qualitatively different from the tropical Pacific and Atlantic. We have therefore chosen not to follow Ji et al.'s (1995) approach.

However, Ji et al. (1995) show an interesting comparison of the observed SST anomalies in the tropical Pacific in November 1991 through April 1992—an ENSO period—with their estimated flux anomalies for the same period (Fig. 16). Dividing the numbers by nearby values of SST anomalies, estimated from the contours, suggests rather greater values of λ' (17-35 $W/m^2/°C$) than the ones obtained by Seager et al (1988) and Kleeman and Power (1995). It would be of interest to examine estimates of λ' from the Ji et al. (1995) approach more thoroughly, using a longer data set.

If these higher tentative estimates of λ' from Ji et al (1995) were confirmed, one would need to explore what is missing in the atmospheric models of Seager et al. (1988) and Kleeman and Power (1995). One possibility is that higher SSTs in the east Pacific tend to imply higher cloud cover, and so less solar radiation. This effect will provide an extra negative feedback, not accounted for in either model. However, note that if an ocean model is run with an observed, interannually-varying shortwave radiation product, such interannual variations in shortwave radiation will be explicitly included. The Seager et al.

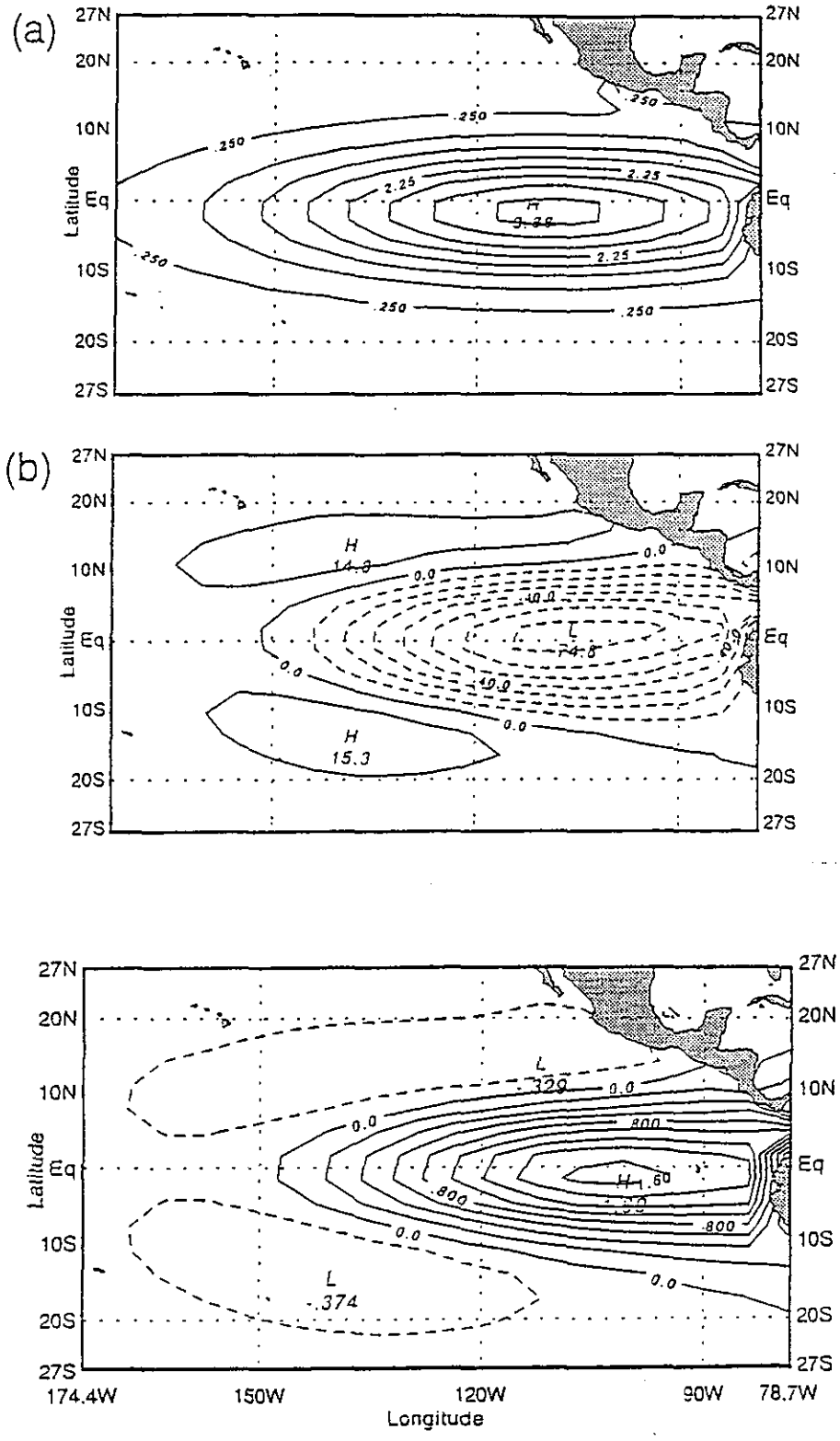

Figure 15a: East Pacific SST anomaly imposed by Kleeman and Power (1995) in their model.

Figure 15b: Net surface heat flux anomaly corresponding to Figure 15a above, from the Kleeman and Power (1995) model.

Figure 15c: Anomaly of air temperature corresponding to Figures 15a,b above, from the Kleeman and Power (1995) model.

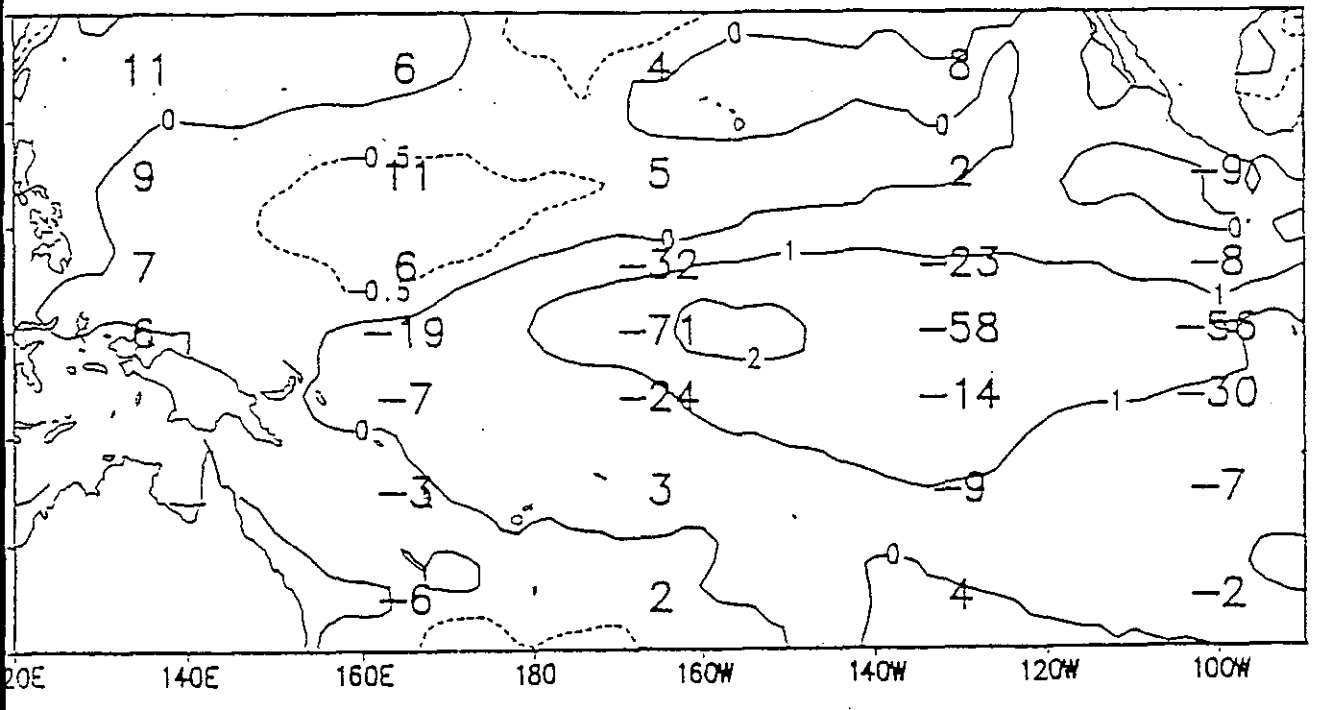

Figure 16: Contours show SST anomaly (°C) for the tropical Pacific for November 1991 through April 1992. The numbers show the corresponding net heat flux anomalies (in W/m^2), estimated from the analysis scheme of Ji et al. (1995). From Ji and Leetmaa (1995).

(1988) or Kleeman and Power (1995) approaches should be adequate for modelling large-scale variations in the other three components of the net heat flux, for which they are designed.

(iii) There have been further modifications of the original method of Seager et al. (1988). Seager and Blumenthal (1994) explored the use of ISCCP (International Satellite Cloud Climatology Project) shortwave radiation products, finding among other things that the ISCCP and ERBE (Earth Radiation Budget Experiment) products differ by 15-25 W/m^2 in the tropics on annual mean. Chen et al. (1994b) used the Seager et al. (1988) method, with minor changes, in their model of seasonal SST in the Pacific Ocean. Their choice of coefficients in (13) were "close to the optimal estimates of Blumenthal and Cane (1989)". Their form for penetrating radiation was somewhat different from others, namely $I(z) = 0.33 * I(0) \exp(-z/h)$, with h = 17 m. The coefficient 0.33 seems rather low. Like Seager and Blumenthal (1994), they used a form of ISCCP short-wave radiation—also a COADS-based product (which was too smooth), and a "fast" product based on ISCCP (that differed from the "bulk" product used by Seager and Blumenthal by about 40 W/m^2!). They drove their model with 3 wind products: FSU, Hellerman and Rosenstein, and an SSM/I product, all with the same bulk transfer coefficient C_D of 0.0015. The FSU winds were consistently lighter than the other two. They do not discuss (P-E) forcing. Of the runs with the three radiation products, the ISCCP "bulk" product (and FSU winds) performed best-though inclusion of penetrating radiation was necessary for this result. SSTs were everywhere higher with the FSU product than with the other two, because of their lower wind speeds.

Of particular relevance to our LWRRDC model, Chen et al. (1994b) describe the results of a "flux correction" experiment, in which a "Haney-type" run was first performed, with an extra term $\lambda_0(T_{model} - T_{obs})$ added to (13); λ_0 was 40 $W/m^2/°C$. The annual mean of $\lambda_0(T_{model} - T_{obs})$ resulting from this run was then added, as a fixed flux correction, to (13) for the next run. The annual mean SST from this experiment agreed very well with observation (as it should). The modelled seasonal cycle of SST was less satisfactory, but adequate. The average magnitude of the flux correction was about 20 W/m^2—small enough to be attributable to errors in the flux algorithms—though the flux correction was in some places substantially larger than 20 W/m^2 (Chen et al. (1994b), Plate 12, 2nd panel)

(iv) Finally, Syu et al. (1995) describe a hybrid coupled model of ENSO phenomena. Their estimate of the surface heat flux is basically that of Seager et al. (1988), though they blend the weak relaxation coefficient λ' inferred from (12) into the Haney (1971) coefficients of Oberhuber (1988), poleward of 20°N,S. They apparently had no (P-E) forcing.

7.2 Heat flux formulation proposed for LWRRDC interannual runs

A major aim of the Division of Marine Research component of the LWRRDC project is to test the ability of our OGCM—when driven with a "state-of-the-art", observation-based estimate of interannual fluxes—to simulate observed interannual SST anomalies. For this purpose, we have

decided to generate an interannually-varying estimate of the net heat flux via the formula (Seager et al. 1988; Chen et al. 1994b):

$$Q_{tot} = R_s + \rho_a C_E L_v W(0.98q_{sat}(T_s) - q_a) + \alpha'(T_s - T^*) + Q_{correct} \qquad (16)$$

where R_s is a satellite-based estimate of short-wave radiation.

The second term in (16) corresponds to latent heat exchange; ρ_a is air density, C_E is bulk transfer coefficient and L_v is latent heat of vaporisation. W is an estimate of wind speed—we will take $W^2 = |\tau| + W_0^2$, where $|\tau|$ is the magnitude of the monthly mean FSU wind pseudostress estimate and W_0 is a "gustiness estimate". We have taken $W_0 = 3\,m\,s^{-1}$, and $C_E = 0.0015$. $q_{sat}(T_s)$ is the saturated water vapour pressure over water at temperature T_s, and q_a an estimate of the air vapour pressure. After some experimentation we chose a pure Seager et al. (1988) approach, with $q_a = \delta q_{sat}(T_s)$. In the main interannual runs, we have used mean seasonal COADS data to estimate δ directly as a function of position and season.

With these choices, the term $\rho_a C_E L_v W|(0.98q_{sat}(T_s) - q_a)$ implies an SST damping rate $\partial Q_{tot}/\partial T_s$ of typically 12 $W/m^2/°C$. According to the discussion in 7.1 above, this may be too small, by perhaps a factor of 50% for spatially extensive SST anomalies and more than this for SST anomalies of smaller spatial scales.

The third term in (16) represents the sum of sensible heat exchange and net longwave radiation, with $\alpha' = 1.5\,W/m^2/°C$. According to the Oberhuber (1988) climatology, this sum is climatologically constant at about 55 W/m^2 over the tropical Pacific and Indian Oceans. We choose $T^* = -8°C$, so that at a typical tropical SST of 27°C, the third term $\alpha'(T_s - T^*)$ is 54 W/m^2. This representation of the sum of sensible heat exchange and long wave radiation is certainly accurate within the errors of order 20 W/m^2 or more in these estimates.

The last term in (16) represents a "flux correction", which must be added because the SST damping rate $\partial Q_{tot}/\partial T_s$ is quite small. We obtain this flux correction by (a) estimating the first three terms of (16) using observed mean seasonal SSTs $T_{Reyn-seas}$ from the Reynolds SST product; (b) running our OGCM with $Q_{correct}$ replaced by $\lambda(T_{model} - T_{Reyn-seas})$, and λ an artificially large damping coefficient of 100 $W/m^2/°C$. This ensures that typical flux errors of up to 50 W/m^2 and typical SST errors of up to 0.5°C will contribute about equally. The resulting estimate of $Q_{correct}$ is stored, and used in (16) for runs to test the OGCM's ability to simulate SST anomalies.

7.3 Use of the IMET time series to test our formulation

The emphasis in the IMET time series is on quite short timescales, rather than the seasonal timescales to be addressed in our runs; and as it is only at one location we cannot address such questions as the adequacy of (16) in the western Indian Ocean. Therefore our tests are quite brief.

(i) The dashed line in Figure 17 shows the difference between modelled and observed values of daily average SST, with the net heat flux estimated from (16) with $Q_{correct} = 0$, and with R_s, wind speeds and SST taken directly from IMET observations. q_a was estimated from (14a). We have taken C_E to be constant at 0.0015. Our use of a "gustiness estimate" of 3.0 ms^{-1} roughly allows for the strong wind-speed dependence of

the bulk transfer coefficient C_E at low wind speeds, in the COARE bulk algorithm. (This approximation yielded latent heat fluxes that differed from the exact values with an rms error of less than 20 W/m^2, and a mean error over the COARE period of about 5 W/m^2.)

A high resolution (2 m grid interval) was used in the model. Evidently, the daily-mean SST difference of Figure 17 (dashed line) is no larger than is obtained with the exact IMET flux data set (Fig. 10), which suggests that (16) is a good proxy for IMET fluxes, when good wind and radiation data are available. The density-based mixed-layer depth (Fig. 18) was quantitatively very similar to that from the exact run (Fig. 7a).

(ii) Different wind speed products (FSU (e. g. Stricherz et al. 1992); Hellerman and Rosenstein1983) differ from one another by up to 20%. The lower full line in Figure 17 shows the (modelled-observed) SST when the observed IMET values of W are reduced by 20%; in all other respects the run was identical to that of (i). This increased the net heat flux into the water by about 20 W/m^2, so the resulting steady 1°C increase in SST is roughly consistent with the 0.5°C rise resulting from a 10 W/m^2 input (Fig. 13).

(iii) Different estimates of shortwave radiation (ISCPP, ERBE, etc.) differ from one another by about 10%, or worse. The upper full line of Figure 17 shows the (modelled-observed) SST when the observed IMET values of R_s are increased by 10%; in all other respects the run was identical to that of (ii) (i.e. wind speed is also reduced relative to (i)). The modeled SST is about 2.5°C warmer than observed, consonant with the flux error of about 40-50 W/m^2.

(iv) To test the effectiveness of our proposed flux correction method for dealing with errors such as those in run (iii), the dotted line in Figure 17 shows the (modelled-observed) SST when the fluxes are those of (iii), with an additional term of $\lambda_0(T_{model} - T_{obs})$. λ_0 was 100 $W/m^2/°C$. We expect a residual SST error of about $(50\ W/m^2)/\lambda_0$ or about 0.5°C. This is in fact generated by the model.

(v) Finally, we tested the effect on daily-averaged SST of replacing the shortwave radiation by its daily mean. This is, of course, a major approximation on an instantaneous basis—R_s can vary from 0 to 1000 W/m^2 over a day, so its replacement by a mean of about 200 W/m^2 could have important effects on the nonlinear mixed-layer behaviour. However, this was not so in the fine-grid model (compare Figure 19a with Figure 5a), nor in the coarse-grid model (compare Figs. 19b, 19c which show results with and without diurnal smoothing). We therefore decided to perform the main LWRRDC runs with monthly mean shortwave radiation, rather than attempting to impose a realistic diurnal variation.

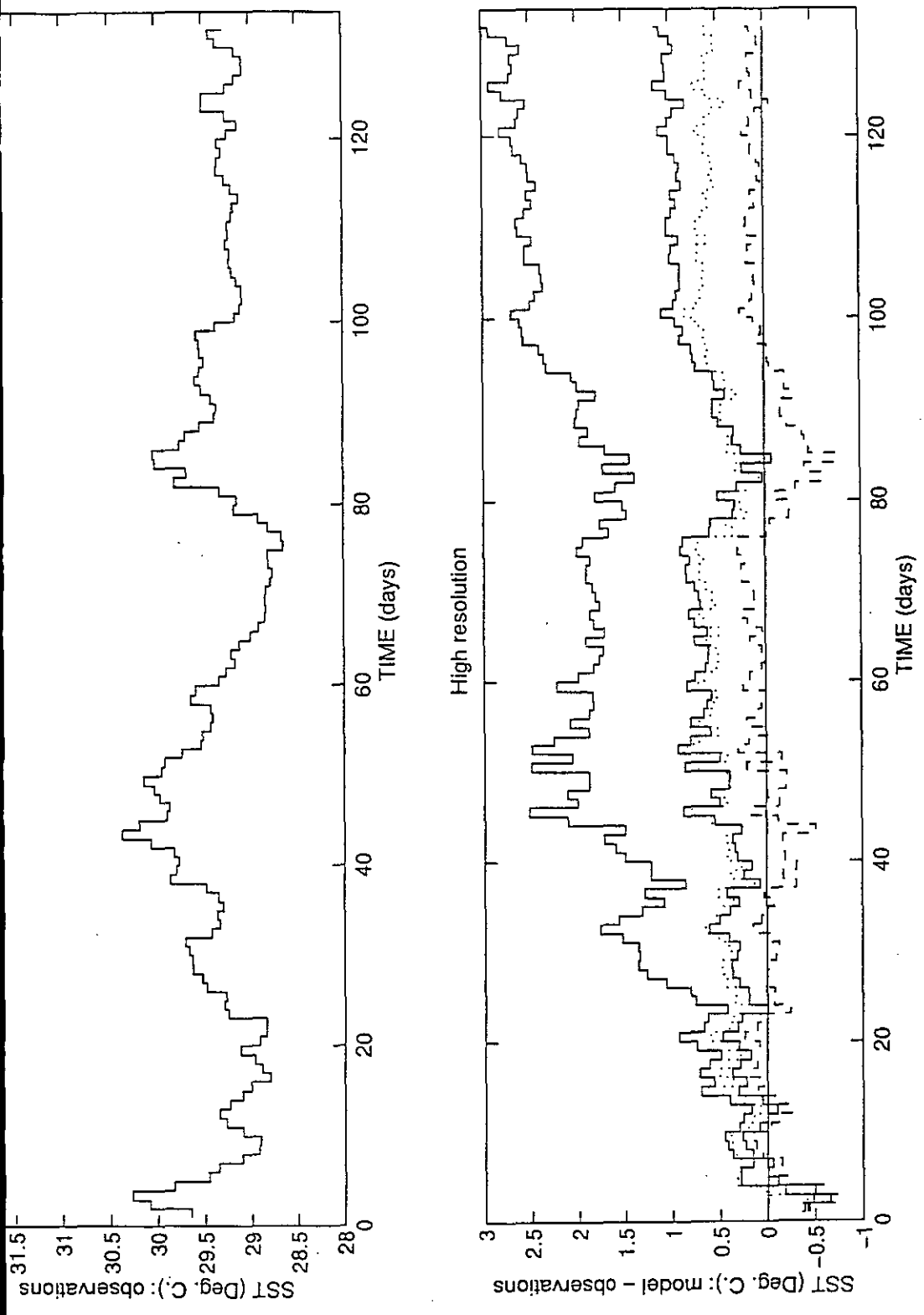

Figure 17: (Modelled-observed) differences in SST between runs with various approximations to the observed IMET flux. Dashed line: flux estimated from (16), with observed R_s and wind speed, and q_a from (14a); $W_0 = 3$ m s^{-1}. Bottom full line: as in dashed line, but with IMET wind speed reduced by 20%. Top full line: as in bottom full line, but with R_s increased by 10%. Dotted line: as in top full line, but with a damping term $\lambda_0(T_{model}-T_{obs})$ added.

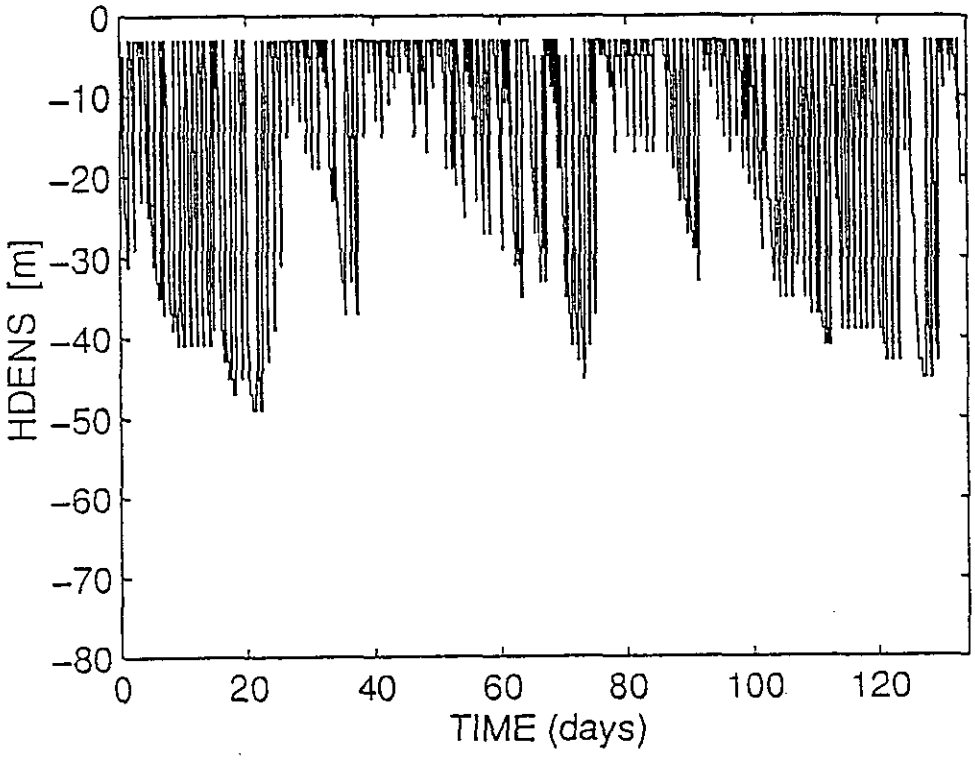

Figure 18: Density-based mixed-layer depth from the first run of Figure 17. Compare with Figure 7a.

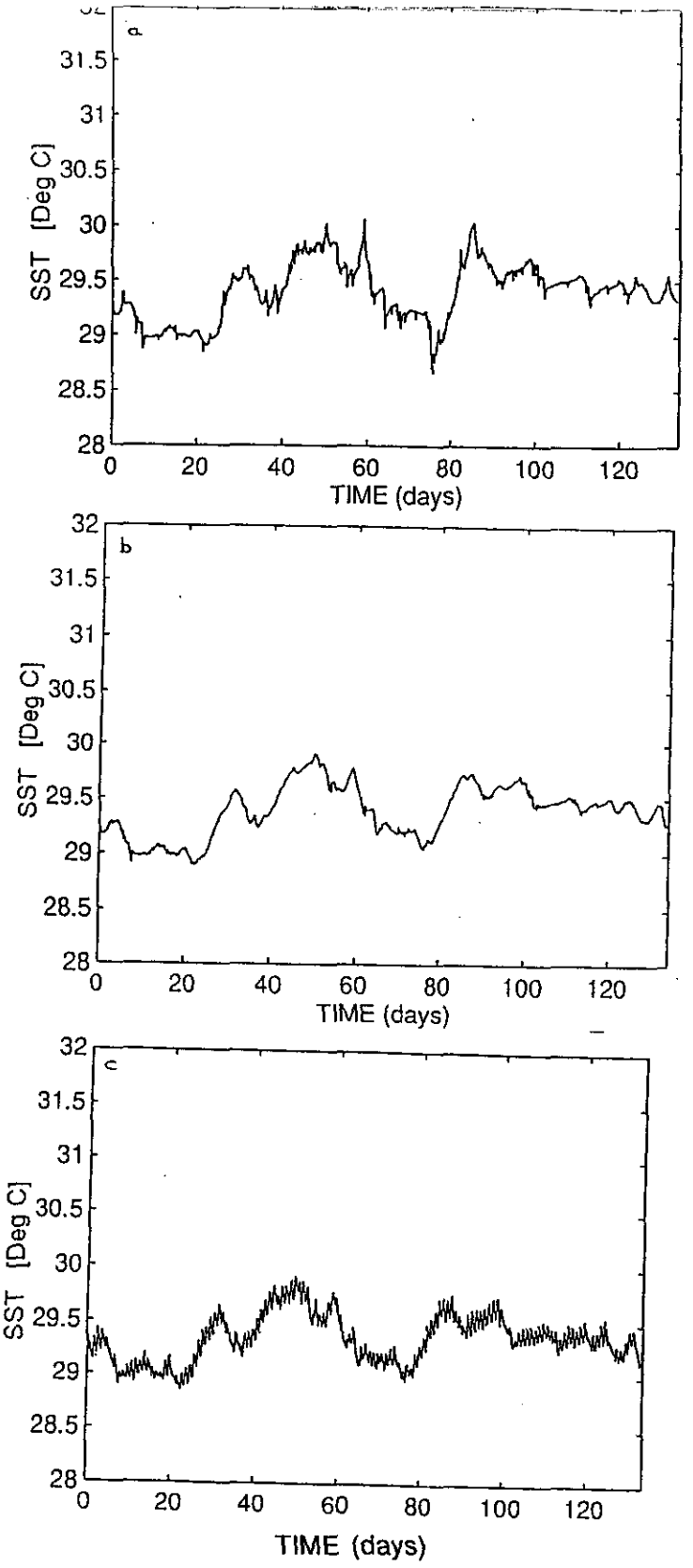

Figure 19: (a) Modelled SST for the fine-resolution run, with R_s replaced by its daily average. Compare with Figure 5a. (b), (c): Modelled SST for the coarse-resolution run (with, without) R_s replaced by its daily average.

REFERENCES

Anderson, S.P., R.A. Weller and R. Lukas (1996). Surface buoyancy forcing and the mixed-layer of the western Pacific warm pool: observations and 1-D model results. *J. Climate*, (submitted).

Cane, M.A., S. Zebiak and R. Dolan (1986). Experimental forecasts of El Nino. *Nature* **321**, 827.

Chen, D., L.M. Rothstein and A.J. Busalacchi (1994a). A hybrid vertical mixing scheme and its application to tropical ocean models. *J. Phys. Oceanog.* **24**, 2156-2179.

Chen, D., A. Busalacchi and L.M. Rothstein (1994b). The roles of vertical mixing, solar radiation, and wind stress in a model simulation of the sea surface temperature seasonal cycle in the tropical Pacific Ocean. *J. Geophys. Res.* **99**, 20345-20359.

Cronin, M.F. and M.J. McPhaden (1996). The upper ocean heat balance in the equatorial Pacific warm pool during September-December 1992. *J. Geophys. Res.* (submitted).

Davis, R.E., R. de Szoeke, D. Halpern and P. Niiler (1981). Variability in the upper ocean during MILE. Part I: The heat and momentum balances. *Deep-Sea Res.* **28A**, 1427-1451.

Feng, M., P. Hacker and R. Lukas (1997). Heat and freshwater balance in the upper ocean in response to WWB during the TOGA COARE intensive observation period. Submitted.

Ffield, A. and A.L. Gordon (1992). Vertical mixing in the Indonesian thermocline. *J. Phys. Oceanogr.* **22**, 184-195.

Godfrey, J.S., M. Nunez, E.F. Bradley, P.A. Coppin and E.J. Lindstrom (1991). On the net surface heat flux into the equatorial western Pacific. *J. Geophys. Res.* **96**, 3391-3400.

Godfrey, J.S., A. Alexiou, A.G. Ilahude, D.M. Legler, M.E. Luther, J.P. McCreary, Jr., G.A. Meyers, K. Mizuno, R.R. Rao, S.R. Shetye, J.H. Toole, S. Wacongne (1995). The Indian Ocean as a component of the global climate system: towards an Indian Ocean component of the Global Ocean Observing System. OOSDP Background Report Number 6.

Godfrey, J.S., R.A. Houze, Jr., R.H. Johnson, R. Lukas, J.-L. Redelsperger, A. Sumi and R. Weller (1997). The Coupled Ocean-Atmosphere Response Experiment (COARE): An interim report. *J. Geophys. Res.* (in press).

Haney, R.L. (1971). Surface boundary condition for Ocean Circulation Models. *J. Phys. Oceanog.* **1**, 241-248.

Hellerman, S. and M. Rosenstein (1983). Normal monthly wind stress over the World Ocean with error estimates. *J. Phys. Oceanog.* **13**, 1093-1104.

Huyer, A., P.M. Kosro, R. O'Malley, and J. Fleischbein (1993). SEASOAR and CTD observations during a COARE surveys cruise, W9211C, 22 January to 22 February 1993. COAS, OSU, Data Report 154, Ref. 93-2, 325 pp.

Huyer, A., P. Hacker, P.M. Kosro, J. Fleischbein, E. Antonissen, and R. O'Malley (1994). SEASOAR and CTD observations during a COARE survey cruise, W9211A, 8 November to 8 December 1992. COAS, OSU, Data Report 155, Ref. 94-1, 364 pp.

Ji, M., A. Leetmaa and J. Derber (1995). An ocean analysis system for seasonal to interannual climate studies. *Mon. Weath. Rev.* **123**, 460-481.

Kleeman, R., and S.B. Power (1995). A simple atmospheric model of surface heat flux for use in ocean modelling studies. *J. Phys. Oceanogr.* **25**, 92-105.

Niiler, P.P. and E.B. Kraus (1977). One-dimensional models. In: Modelling and Prediction of the Upper Layers of the Ocean, E.B. Kraus (Ed.). Pergamon Press.

Oberhuber, J.M. (1988). An atlas based on the COADS data set: the budgets of heat, buoyancy and turbulent kinetic energy at the surface of the global ocean. Max-Planck Institut fur Meteorologie Report No. 15.

O'Malley, R., P.M. Kosro, R. Lukas, and A. Huyer (1994). SEASOAR observations during a COARE survey cruise, W9211B, 12 December 1992 to16 January 1993. COAS, OSU, Data Report 156, Ref. 94-2, 426 pp.

Pacanowski, R.C. (1995). MOM2 Documentation User's Guide and Reference Manual, version 1.0. GFDL Technical Report 3.

Pacanowski, R. and S.G.H. Philander (1981). Parameterisation of vertical mixing in numerical models of tropical oceans. *J. Phys. Oceanog.* **11**, 1443-1451.

Peters, H., M.C. Gregg, and J.M. Toole (1988). On the parameterization of equatorial turbulence. *J. Geophys. Res.* **93**, 1199-1218.

Power, S.B., R. Kleeman, F. Tseitkin and N.R. Smith (1995). On a global version of the GFDL Modular Ocean Model for ENSO studies. BMRC Technical Report, October 1995.

Price, J., R. Weller and R. Pinkel (1986). Diurnal cycling: observations and models of upper ocean response to diurnal heating, cooling and wind mixing. *J. Geophys. Res.* **91**, 8411-8427.

Seager, R., S.E. Zebiak, and M.A. Cane (1988). A model of the tropical Pacific sea surface climatology. *J. Geophys. Res.* **93**, 1265-1280.

Seager, R., and M.B. Blumenthal (1994). Modeling tropical Pacific sea surface temperature with satellite-derived solar radiative forcing. *J. Climate* **7**, 1943-1957.

Siegel, D.A., J.C. Ohlmann, L. Washburn, R.D. Bidigare, C.T. Nosse, E. Fields and Y. Zhou (1995). Solar radiation, phytoplankton pigments and the radiant heating of the equatorial Pacific warm pool. *J. Geophys. Res.* **100**, 4885-4891.

Smyth, W.D., D. Hebert and J.N. Moum (1996). Local ocean response to a multiphase westerly windburst. Part 2: Thermal and freshwater response. *J. Geophys. Res.* (in press).

Stricherz, J.N., J.J. O'Brien and D.M. Legler (1992). Atlas of Florida State University tropical Pacific winds for TOGA 1966-1985. Florida State University, 256 pp.

Syu, H.-H., J.D. Neelin and D. Gutzler (1995). Seasonal and interannual variability in a hybrid coupled GCM. *J. Climate* **8**, 2121-2143.

Wacongne, S. and R. Pacanowski (1996). Seasonal heat transport in a nonlinear primitive equation model of the Indian Ocean. *J. Geophys. Res.* (in press).

Waterman, L. (m/s in preparation).

Weare, B.C., P.T. Strub and M.D. Samuel (1981). Annual mean surface heat fluxes in the tropical Pacific Ocean. *J. Phys. Oceanog.* **11**, 705-717.

Weller, R.A. and S.P. Anderson (1996). Surface meteorology and air-sea fluxes in the western equatorial Pacific warm pool during the TOGA Coupled Ocean-Atmosphere Response Experiment. *J. Climate* (in press).

Vertical Structure			
k	*mid-depth*	*level thickness*	*depth of bottom*
1	7.5	15.00	15.00
2	22.5	15.00	30.00
3	37.5	15.00	45.00
4	52.5	15.00	60.00
5	67.5	15.00	75.00
6	82.5	15.00	90.00
7	97.5	15.00	105.00
8	112.5	15.00	120.00
9	127.5	15.12	135.12
10	142.74	15.44	150.56
11	158.38	16.19	166.75
12	175.12	17.91	184.66
13	194.20	21.57	206.23
14	218.26	28.86	235.09
15	251.92	42.48	277.57
16	303.22	66.28	343.85
17	384.48	105.12	448.97
18	513.46	164.22	613.19
19	712.92	247.83	861.02
20	1009.12	357.34	1218.36
21	1427.60	489.36	1707.72
22	1987.84	634.44	2342.16
23	2696.48	777.32	3119.48
24	3542.48	899.14	4018.62
25	4494.76	981.38	5000.00

Table 1: Vertical T-grid: mid-depth, level thickness and depth at the bottom of each level (m).

CSIRO Marine Laboratories

Division of Marine Research
(formerly the Division of Fisheries and the Division of Oceanography)

Headquarters
Castray Esplanade, Hobart, Tasmania 7001
GPO Box 1538, Hobart, Tasmania 7001, Australia

Queensland Laboratory
133 Middle Street, Cleveland, Queensland 4163
PO Box 120, Cleveland, Queensland 4163, Australia

Western Australia Laboratory
Leach Street, Marmion, W.A.
PO Box 20, North Beach, W.A. 6020, Australia

ISBN 0 643 06157 6
ISSN 0725–4598